Original Paper

Landslides
DOI 10.1007/s10346-022-02004-4
Received: 1 August 2022
Accepted: 28 November 2022

O. Adrian Pfiffner · Susan Ivy-Ochs · Zhasmin Mussina · Jordan Aaron · Olivia Steinemann · Christof Vockenhuber · Naki Akçar

The Tamins rock avalanche (eastern Switzerland): timing and emplacement processes

Abstract The Tamins rock avalanche lies adjacent to the Flims rock avalanche, the largest in the Alps. Its deposit forms a ridge across the Rhine Valley just downstream of the confluence of the Vorderrhein and Hinterrhein rivers. The deposit is dominated by a 1.6-km-long longitudinal ridge, Ils Aults, and two roughly 600-m-long transverse ridges. Several extensional scarps bear witness to spreading of the deposit. A breach through the deposit, where the Rhine River presently flows, reveals a carapace and intense fragmentation. Exposure dating using cosmogenic ^{36}Cl yields an age of 9420 ± 880 years. This suggests that the Tamins event occurred in a time frame similar to the Flims event but was slightly earlier than the Flims rock avalanche, as also required by stratigraphic relationships. 3D volume modeling reveals bulking of only 14%. The motion of the rock avalanche seems to have occurred first as a flexible block, which underwent fragmentation and simple shearing where the top moved faster than the bottom. The ensuing spreading led to the formation of extensional scarps. There is no identified weak layer along the sliding surface; nevertheless, modeling suggests a friction angle of 10°.

Keywords Rock avalanches · Tamins rock avalanche · Morphology of rock avalanches · Cosmogenic nuclide dating · Numerical modeling of rock avalanches

Introduction

Rock avalanches dramatically modify landscapes over short timescales. In mountainous regions, rock avalanches can dam rivers which often leads to the formation of lakes. Overtopping and/or breaching of these dams can result in major floods (Costa and Schuster 1988; Fan et al. 2020; Argentin et al. 2021). Catastrophic events like rock avalanches, associated debris flows and outbreak of lakes represent considerable hazard to people (Schwinner 1912; Heim 1932; Abele 1974; Hovius et al. 1997).

A better understanding of rock avalanche occurrence and motion requires detailed analysis of a large number of case histories (e.g., Evans et al. 1994; Nagelisen et al. 2015; Grämiger et al. 2016; Ivy-Ochs et al. 2017; Singeisen et al. 2020). As rock avalanches are infrequent events, studies of pre-historic rock avalanches provide crucial information regarding rock avalanche geomorphology and sedimentology (e.g., Cruden and Hungr 1986; Giorgio et al. 1991; Dufresne et al. 2016), runout mechanisms (e.g., Evans et al. 1994; Nagelisen et al. 2015; Castleton et al. 2016; Grämiger et al. 2016; Aaron et al. 2020), and temporal occurrence (e.g., Ivy-Ochs et al. 2017; Ruggia et al. 2021), especially for the rare extreme volume event. In particular, detailed mapping of prehistoric rock avalanches has revealed that the source zone stratigraphy often remains intact in the highly comminuted deposit (e.g., Strom 2006, Dufresne et al. 2016; Singeisen et al. 2020; Pfiffner 2022). Furthermore, rock avalanche deposits typically feature a boulder-rich carapace, which is underlain by a highly fragmented body facies. The base of rock avalanche deposits often features evidence of mixing with path material that is overridden during the event (Weidinger et al. 2014; Dufresne et al. 2016; Rossato et al. 2020).

Runout analyses of prehistoric rock avalanches have revealed important information regarding geomorphic interpretations of rock avalanche landforms (e.g., von Wartburg et al. 2020), the role of path material in controlling rock avalanche dynamics (Hungr and Evans 2004; Aaron and McDougall 2019), and the ultimate strengths (defined as the bulk basal resistance after 10's of meters of displacement) required in the source zone for catastrophic failure to occur. In particular, Aaron and McDougall (2019) suggest that a volume-dependent mechanism must reduce the basal resistance in the source zone, and that this contributes to the well-known volume dependence of rock avalanche mobility (Scheidegger, 1973). However, further case histories are required to better understand and confirm this trend.

Finally, dating of pre-historic events is crucial for understanding failure sequences, and placing rock avalanche occurrence in a regional context. Prior to being dated, the deposits of many events have been erroneously interpreted as having resulted from multiple failures (e.g., Ivy-Ochs et al. 2017; von Wartburg et al. 2020). Further, the timing of rock avalanche occurrence relative to deglaciation has been controversial, although much recent progress has been made (e.g., Hermanns and Longva 2012; Ballantyne et al. 2014; Ivy-Ochs et al. 2017).

These aspects are well demonstrated by two remarkable rock avalanches which are located near the confluence of the Vorderrhein and Hinterrhein branches of the Rhine River in eastern Switzerland (Fig. 1): the Tamins and the Flims rock avalanches. The Flims rock avalanche, with a volume of 11–11.5 km^3 (Caprez 2008; Pfiffner 2022) is the largest in the Alps, and has received considerable interest in the past 200 years, while the Tamins rock avalanche, which is the subject of the present work, has played a comparatively minor role in research activity.

The Tamins rock avalanche was initially considered to be part of the Flims rock avalanche (Heim 1883; Hartung 1884), until Piperoff (1897) and Staub (1910) mapped the area in detail and recognized the Tamins rock avalanche as a separate unit. The Flims rock avalanche mobilized the late- and post-glacial sediment upon impacting the valley floor (Abele 1974; Poschinger and Kippel 2009; Calhoun and Clague 2018) and impinged on the

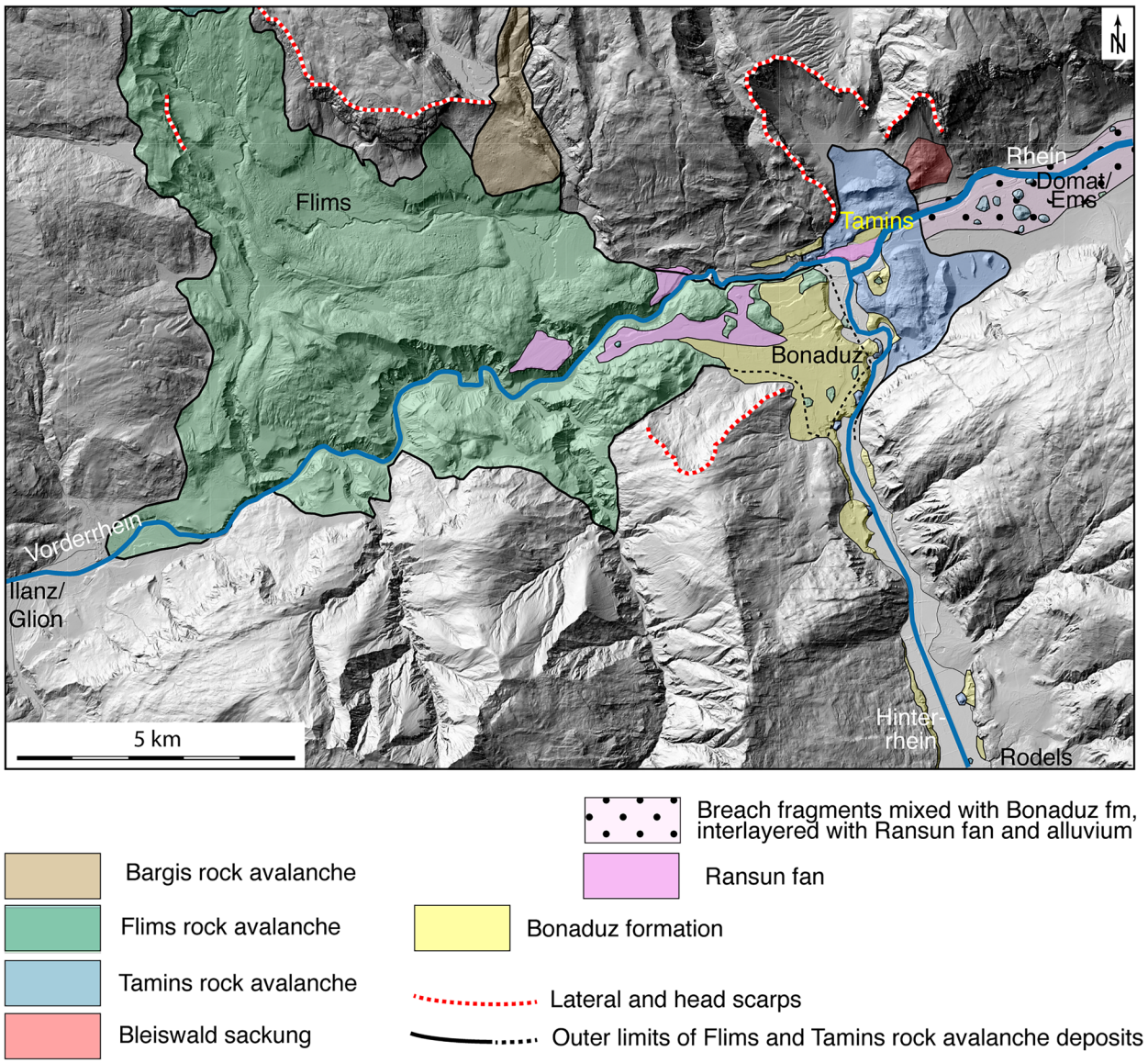

Fig. 1 Digital elevation model of the study area with breakaway scarps, rock avalanche, and associated deposits

Tamins rock avalanche deposit (see also below). The resulting sedimentary complex is referred to as the Bonaduz formation (Fig. 1). Outburst of a lake dammed by the Flims rock avalanche (Ilanzersee) is recorded in the Ransun fan shown in Fig. 1.

A major issue in the research history concerned the question of how long after the Last Glacial Maximum (LGM) the rock avalanches occurred or even if the deposits were overrun by Lateglacial glacier advances (Staub 1910; Oberholzer 1933; Abele 1974; Nabholz 1975). The discussion emerged because of the presence of erratic blocks and striated clasts often in matrix-supported diamictons within and on top of the rock avalanche deposits (v. Poschinger and Haas 1997 and references therein). The Flims rock avalanche has been dated by Deplazes et al. (2007) with the 14C method to 9475–9343 cal BP (recalculated in Nicolussi et al. 2015) and Ivy-Ochs et al. (2009) using cosmogenic ^{36}Cl to 8900 ± 700 years.

The present work includes dating the Tamins rock avalanche, analyzing its morphology, internal structure, and modeling its runout using modern tools (Mussina 2021). The paper is structured as follows. First, an overview of the geology, geomorphology, internal structure, and volume reconstruction of the rock avalanche is given. Next, the results of cosmogenic nuclide dating of boulders in the deposit, as well as a runout analysis of the event, are presented. Finally, all these analyses are integrated to provide a description of the initiation and runout of this event.

Geological framework

The Tamins rock avalanche covers the tectonic boundary between the Helvetic and Penninic nappe systems (Fig. 2). The Helvetic nappe system is subdivided into the Lower and Upper Helvetics. The Lower Helvetics outcrop to the north of the Rhine Valley and

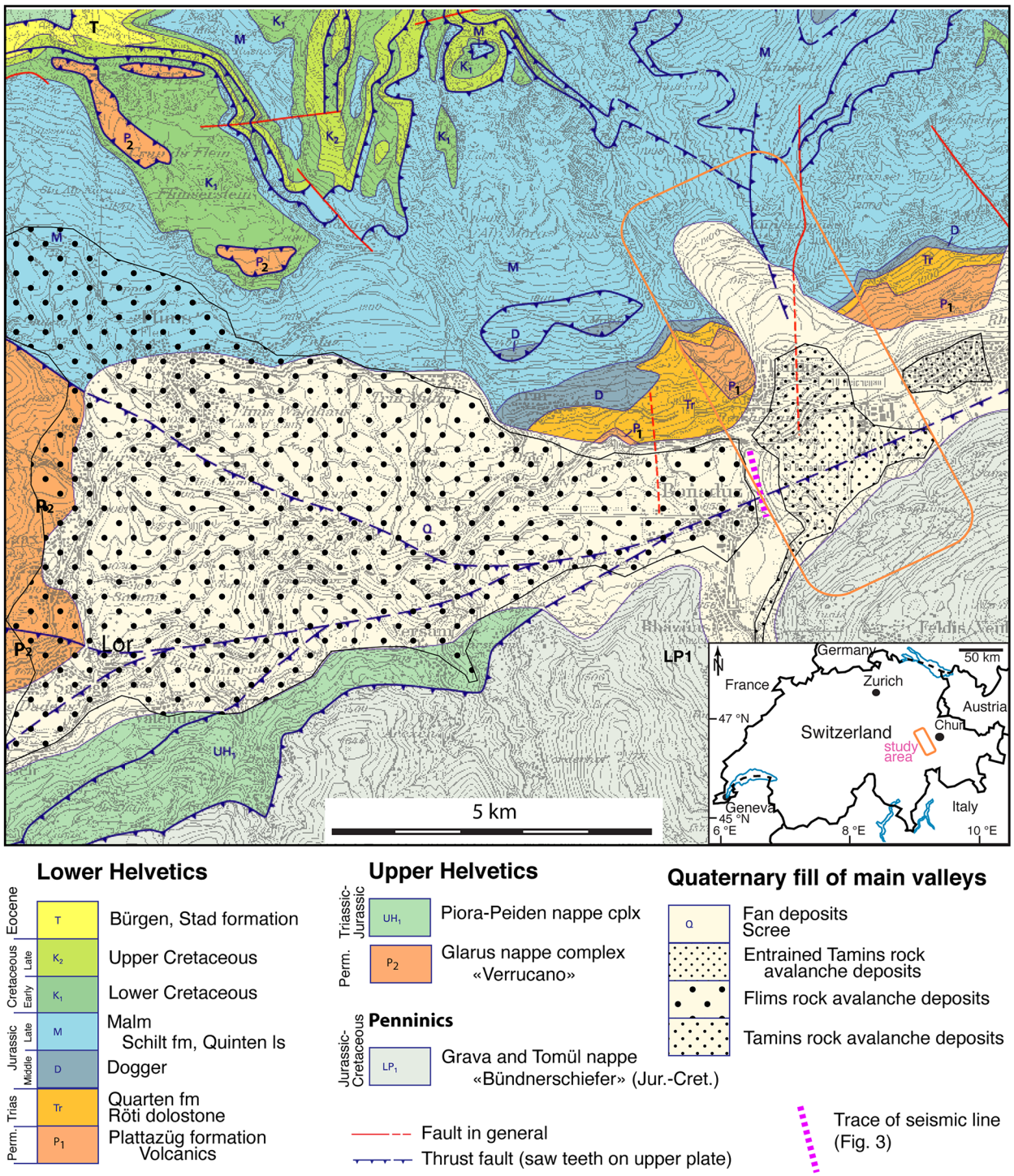

Fig. 2 Geological map of the study area including the Flims rock avalanche. Modified from Pfiffner et al. (2010)

are dominated by the Late Jurassic Quinten limestone building high cliffs. The Upper Helvetics are concealed by the Quaternary valley fill but outcrop farther to the west and northeast. In the map of Fig. 2, they are shown to pinch out toward the study area. The Penninic nappe system outcropping south of the Rhine Valley is made of a thick sequence of shale, marl, and thin-bedded sandstone and limestone (also referred to as "Bündnerschiefer").

The study area lies within the Tschep nappe of the Lower Helvetics. This nappe consists of Jurassic Quinten limestone in the north, which also contains the head scarp of the Tamins rock avalanche. A N-S oriented fault zone (Kunkelspass fault zone) is made up of a vertical fault and a west-verging thrust fault that cuts across the Tschep nappe (Pfiffner 1972a, b). The limestone between the two faults is highly shattered. Permian volcanics (Plattazüg formation) form a large-scale anticline and are enveloped by Triassic dolostone and Jurassic sandstone (Dogger). This fold may be mapped on either side of the Kunkelspass fault zone; its fold axis trends ENE-WSE. The shale, marl, sandstone, and limestone sequence ("Bündnerschiefer") in the south of the study area are affected by decimeter-scaled nearly isoclinal folds with bedding and the main foliation dipping with around 30° to the SSE (Pfiffner 1977, 1978).

Figure 1 shows the major features of the Tamins rock avalanche. The head scarp is horseshoe shaped with two parallel-oriented side scarps that indicate the direction of motion of the rock avalanche. The rock avalanche deposits extend across the Rhine Valley forming a large ridge parallel to the motion direction south of the Rhine and ridges perpendicular to the motion direction north of the Rhine.

As is evident in Fig. 1, the valley floor in the Bonaduz and Domat/Ems region is flat (650 m a.s.l. near Bonaduz, 600 m a.s.l. near Domat/Ems) but is dotted with numerous conical-shaped hills. These hills are called "tuma" in the local language, but are referred to as "toma" in the old literature. They are made of rock avalanche material (Piperoff 1897; Staub 1910; Remenyik 1959, Pfiffner and Wyss in press) and will not be discussed here in more detail. But an important question emerges regarding the valley fill itself. The Rhine Valley is markedly glacially overdeepened with the bedrock top surface at around sea level near Chur (Wildi 1984; Eberle 1987; Pfiffner et al. 1997; Schälli 2012; Zwahlen 2021) and around 100 m a.s.l. near Reichenau (Fig. 3). In the course of deglaciation silt and sand lake and delta sediments accumulated and filled the valley to a level of around 420 m a.s.l., as witnessed by several cores located downstream of Reichenau (Eberle 1987, Müller 1999). These sediments are overlain by coarse-grained clastics (Müller 1999; Zwahlen 2021) that were shed from the flanks of the waning glaciers, from collapsing kames, and from tributary creeks. Extrapolating upstream in the Rhine Valley from Lake Constance, it is reasonable to postulate that the valley floor was at around 500 m a.s.l. at Reichenau just prior to the Tamins rock avalanche event.

The Tamins rock avalanche deposits dammed the Vorder- and Hinterrhein rivers, the dam attained a maximum altitude of 680 m a.s.l. The emerging lake, Lake Bonaduz, extended more than 10 km upstream in the valleys of the two rivers. The Flims rock avalanche crashed into this lake and the sediments at its bottom. The latter were liquefied and accumulated behind the Tamins rock avalanche deposit and were diverted upstream into the Hinterrhein Valley (Nabholz 1975). As an effect of this, the valley floor around Bonaduz was raised from 500 to 650 m a.s.l. (Pfiffner 2022). The Bonaduz formation

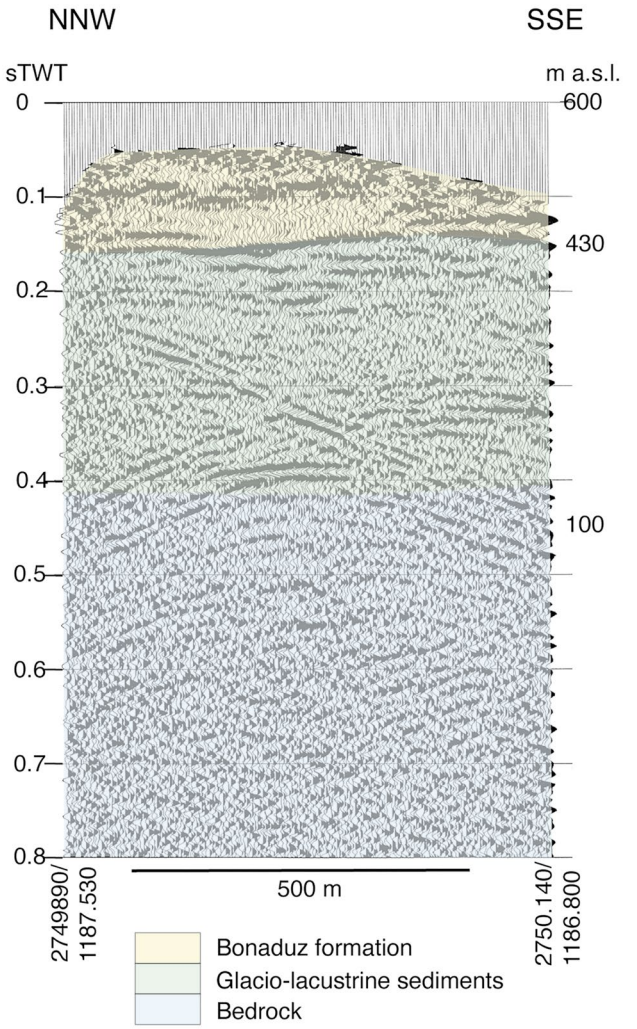

Fig. 3 Seismic reflection line at Bonaduz illustrating the sedimentary fill of the glacially overdeepened valley. Modified from Pfiffner et al. (1997) and Pfiffner and Wyss (in press)

overlies the Tamins rock avalanche deposit at several places, a fact that indicates a relative older age of the Tamins compared to the Flims rock avalanche. Calhoun and Clague (2018) give a detailed account on the nature of the Bonaduz formation, which will not be discussed in more detail here. In the seismic section shown in Fig. 3, the base of the Bonaduz formation is taken to be at 430 m a.s.l. The reflections beneath 0.15 s TWT stem from glacilacustrine sediments according to boreholes 2 km west and 11 km east of the seismic line. The sediments between 430 and 500 m a.s.l. which were transformed into the Bonaduz formation yielded gravel-sized components as well as rip-up clasts of lacustrine silt (see v. Poschinger and Kippel 2009).

Geomorphology of the rock avalanche deposit

More than 100-m-high cliffs outline the head and lateral scarps (Fig. 4A and Fig. 5B). The head scarp extends from Säsagit to Garschlichopf, the two lateral scarps from Säsagit to Vorgelstein and from Garschlichopf to Foppastein. In front of Säsagit, a limestone tower, called Turm (Fig. 4B), is a remnant of the source rock and witnesses the collapse in

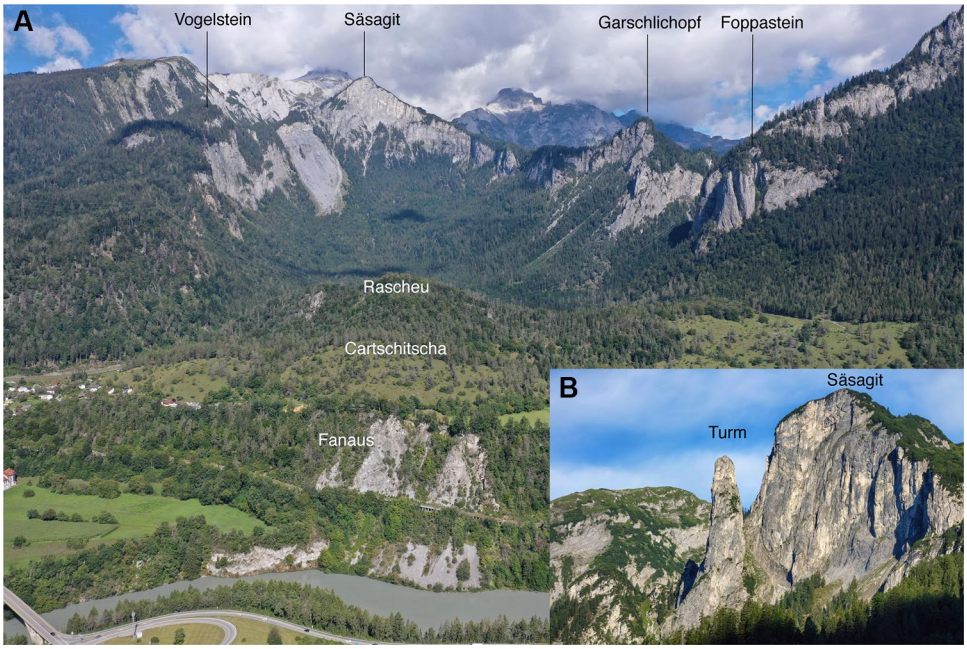

Fig. 4 View of the release area. **A** Head scarp and rock avalanche deposit; Drone photo N. Akçar. **B** Head scarp with remnant of source rock. Photo R. Gertsch

the detachment zone. The forest beneath the cliffs of Säsagit-Vogelstein is the depletion area where the bedrock of the basal detachment surface is locally exposed or is covered by a thin veneer of rock avalanche debris. The accumulation area has two transverse ridges, Rascheu and Cartschitscha (see Fig. 4A and Fig. 5B). The outcrop at Fanaus is the northern flank of the Reichenau breach through the Tamins rock avalanche. To the south of the Rhine River, the linear ridges of Ils Aults, Crest'Aulta and Tuma Lunga dominate the rock avalanche deposits. Numerous hummocks with diameters around 100 m are found dispersed throughout the rock avalanche deposit.

The lithologic composition and geomorphology of the rock avalanche deposit are displayed in Fig. 5. Figure 5A shows the distribution of the boulder lithologies obtained from detailed field mapping. Late Jurassic Quinten limestone is the dominant lithology, coherent with the composition of the source area. Clasts and boulders of older rocks, like Permian volcanics (Plattazüg formation), Triassic dolostone, and Middle Jurassic sandstone, are encountered along the lower part of the western margin of the deposit. Further to the west, Cretaceous limestones pertaining to hills of the Flims rock avalanche deposit emerge through the Bonaduz formation. The Bleiswald sackung to the east of the Tamins rock avalanche (see Fig. 5A) is an earlier feature (Pfiffner and Wyss in press). Here, the Permian and Triassic rocks were moved downward for several hundred meters. The Tamins rock avalanche then swept over it and entrained only Late Jurassic Quinten limestone which is now found in the eastern margin of the Tamins rock avalanche deposit.

Two prominent transverse ridges, Rascheu and Cartschitscha, dominate the morphology north of the Rhine River (Fig. 5B and Fig. 6). For both, the southern flank is steeper than the northern flank (32° versus 26° for Rascheu, 24° versus 7° for Cartschitscha). This suggests that the transverse ridges are extensional features although they are located in the proximal accumulation area. Their flanks are therefore considered as extensional scarps. An important erosional scarp just north of the Rhine River marks the Reichenau breach. A number of 100-m-sized closed basins may be identified in this northern sector (Fig. 6). These basins contain rounded clasts of crystalline rocks, which are totally foreign to the rock avalanche deposit. They stem from a tsunami triggered by the Flims rock avalanche that spilled over the Tamins rock avalanche deposit. Scholz (2018) analyzed this splash zone in detail and could show that splash zone sediments occupy the areas around the closed basins. The pebble spectrum is large. But the most interesting clasts are green and red granites and red breccias. They represent granites from the Austroalpine nappes (Julier granite) and unmetamorphosed Verrucano, which is also typical for the Austroalpine nappes, respectively. Thus, the source of the splash zone must be sought in the Bonaduz formation, which contains clasts from the Hinterrhein (Austroalpine nappes) and the Vorderrhein (gray limestone from the Lower Helvetics). Many of the clasts can be attributed to the Penninic nappes which outcrop along both rivers, while quartz pebbles derived from Alpine quartz veins are inconclusive regarding their origin. Finally, the micromorphology is characterized by meter to 10-m scale depressions and elevations resulting in the hummocky structure of the surface viewed on a DEM by swisstopo with a resolution of 2 m.

South of the Rhine River, the rock avalanche deposit forms a broad longitudinal ridge from Tuma da Zislis to Ils Aults (Fig. 5B and Fig. 6). To the east of Ils Aults, several N-S oriented ridges (for example, Crest'Aulta and Tuma Lunga) stand out of the alluvial plain. The slopes of these ridges are steeper on the eastern flank compared to the western flank (37° versus 11° for Crest'Aulta, 33° versus 27° for Tuma Lunga). We interpret the ridge crests and steep flanks as extensional scarps that reflect the spreading of the rock avalanche as it hit the main valley flank to the south. Several extensional scarps with minor offsets can be recognized immediately east of Ils Aults; they were already reported by Calhoun and Clague (2018). The depression between Ils Aults and Crest'Aulta contains three closed basins. The slope just west of these basins is particularly steep and suggests an extensional scarp from which the rock avalanche deposit drifted away to the east. A number of lineaments with minor morphologic expression cut across Ils Aults (Fig. 6).

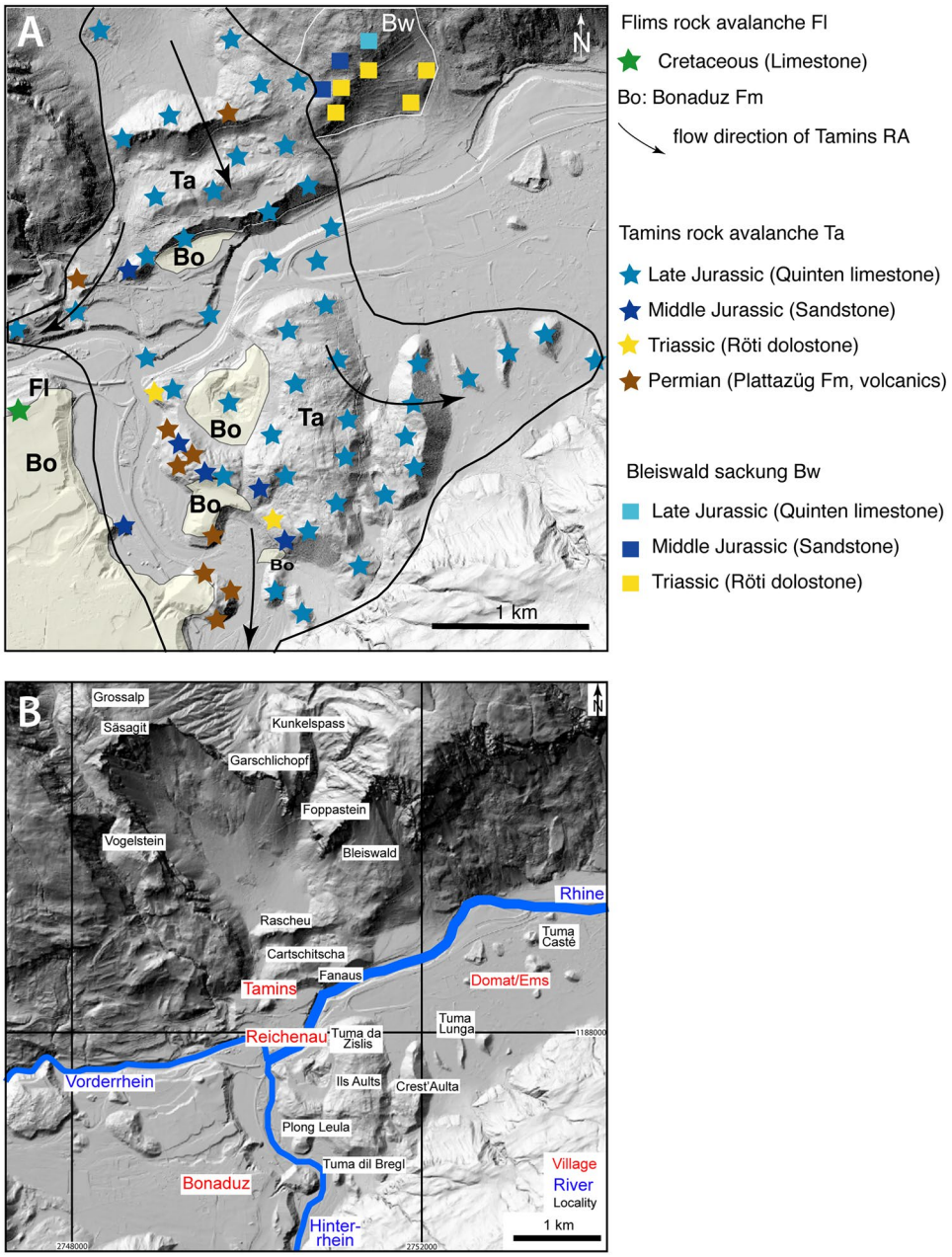

Fig. 5 Digital elevation model (2-m resolution; swisstopo) of the rock avalanche deposit. **A** Distribution of lithologies within the deposit. **B** Geographic map containing locality names

Particularly evident are those just south of Tuma da Zislis. The significance of these lineaments is at present not clear. Diamict deposits with rounded pebbles of diverse lithologies embedded in a silty matrix occur at several locations on top of the longitudinal ridge and suggest that the tsunami triggered by the Flims rock avalanche swept across the longitudinal ridge of the Tamins rock avalanche deposit.

The erosional scarp north of Tuma da Zislis corresponds to the southern flank of the Reichenau breach. Surprisingly, rounded clasts of crystalline rocks are preserved on the steep scarp surface (Fig. 5C). West of the main longitudinal ridge erosional scarps witness incision of the Hinterrhein into the flat-topped Bonaduz formation. The Bonaduz formation is seen to overly the Tamins rock avalanche deposit on both sides of the Hinterrhein SSW of Ils Aults. Additionally, an outcrop of rock avalanche deposit was unearthed beneath the Bonaduz formation in the gravel pit of Reichenau (Fig. 6). It thus follows that the Bonaduz formation and the Flims rock avalanche that triggered it are younger than the Tamins rock avalanche.

Critically, the morphology of the rock avalanche deposits with meter-scale blocks sticking out of the ground and meter-sized closed depressions not filled by till clearly speaks against the passing of a glacier. Singular erratic blocks and small patches of till may well derive from the pre-event topography given that during the LGM the ice surface was well above 2000 m a.s.l.

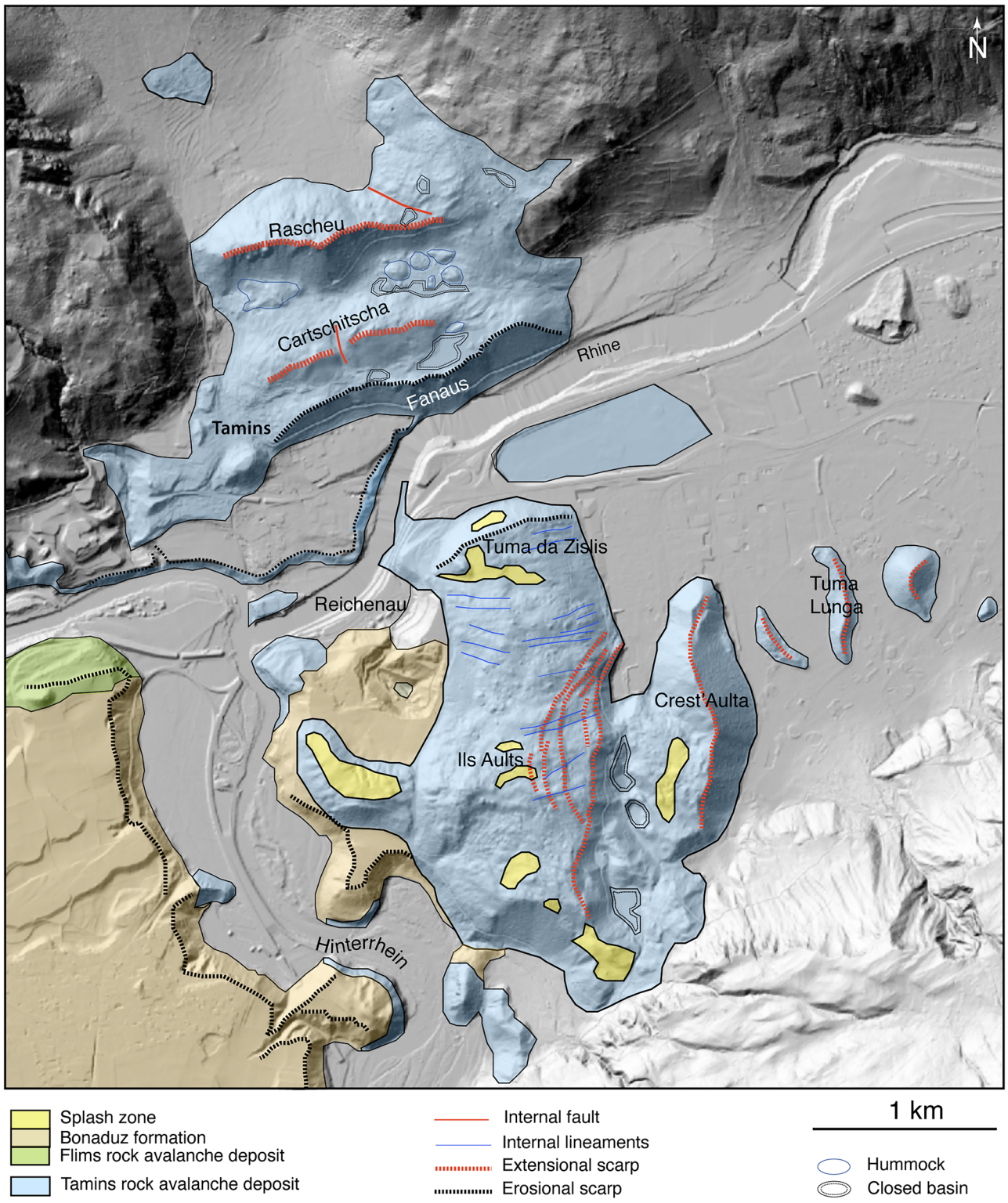

Fig. 6 Digital elevation model of the rock avalanche deposit with morphologic features within the Tamins rock avalanche deposit

Internal structure of the rock avalanche

The Tamins rock avalanche deposit is densely covered by vegetation. Outcrops were created by incision of the Hinterrhein and the Rhine river, and by local construction work. The photograph in Fig. 7 displays meter-sized blocks at the top of the outcrop which pertain to the carapace of the rock avalanche deposit. Beneath these blocks finely crushed limestone containing smaller blocks are part of the main body of the deposit and witness the intense fragmentation.

By far the best insight into the internal structure can be gained in the outcrop of Fanaus located north of the Rhine River in the erosional scarp of the Reichenau breach (location shown in Fig. 5B). The photograph in Fig. 8 gives an overview of the outcrop and segments A to C (Mussina 2021). These segments are shown as photograph and line drawings in Fig. 9A–C. In segment A, the original bedding is preserved over much of the area displayed in Fig. 9A. Bedding is also highlighted by brightly colored massive limestone layers, which are interlayered with gray highly fractured limestone. All in all, we are dealing with a large block that remained coherent at the large scale but was fractured at the small scale. A detailed view of the (inherited) bedding planes is given in Fig. 10A. In segment B, which is located immediately above segment A, traces of bedding are almost obliterated but parallel to the one in segment A (see Fig. 9B). The outcrop displays a more blocky texture where individual blocks are clearly separated from neighboring blocks of similar size. The spaced joints between neighboring blocks suggest enhanced dilation, an observation typical for the carapace of rock avalanches (Weidinger et al. 2014; Dufresne et al. 2016). A detailed view of the blocky texture with jigsaw pattern is given in Fig. 10B. Segment C in Fig. 9C is at the top of the Fanaus outcrop. Large blocks are embedded in smaller fragments and the entire outcrop has a blocky texture reminiscent of a carapace where dilation separated larger blocks and allowed for some rotations. Signs of bedding are not obvious in this segment. As outlined in the line drawing, there is a highly fractured gray limestone layer underlying larger light-colored blocks, the boundary of which might represent an original bedding surface. From Fig. 9A–C, a transition from a coherent block to a blocky texture may be recognized. Interestingly, the original bedding retains the same orientation and suggests that a large block in the rock avalanche experienced more fracturing and dilation upward toward the surface of the rock avalanche. This is held to mark the transition from the interior of the rock avalanche to the carapace (cf. Weidinger et al. 2014). This boundary is schematically labeled in the photograph of Fig. 8.

An abandoned quarry NW of Plong Leula (coord. 2750.530/1187.030 of the national Swiss km grid) provides insight into the Tamins rock avalanche deposits which here consist of Permian volcanics (Plattazüg formation). The carapace nature is evident from the randomly oriented schistosity within the individual angular blocks (see Fig. 10C). The close-up in Fig. 10D displays small fragments nested between the larger blocks. Open spaces between the larger blocks witness dilation, but are filled with comminuted rock.

A remarkable outcrop is located in the erosional scarp of the Hinterrhein at Tuma dil Bregl (coord. 2751.000/1186.340; see Fig. 5B), which was already described in detail by Calhoun and Clague (2018)

Fig. 7 Outcrop of rock avalanche deposits in the north of Crest'Aulta (coord. 2752.000/1187.800; see Fig. 5B)). Large blocks of limestone at the top of the outcrop rest on finely crushed limestone beneath. Photo A. Pfiffner

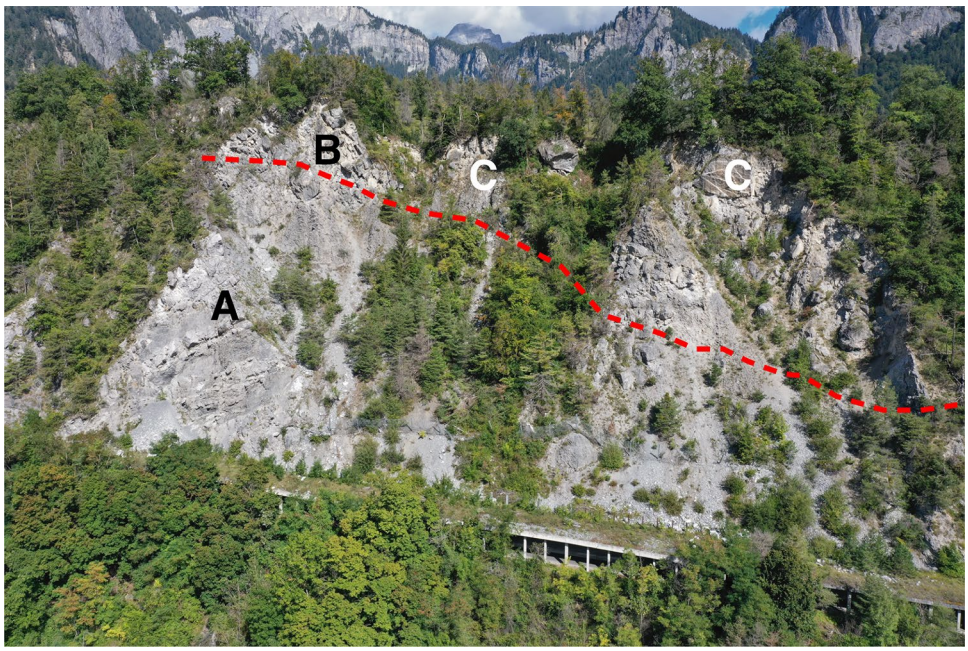

Fig. 8 Overview of the outcrop Fanaus in the erosional scarp of the Reichenau breach. **A**, **B**, and **C** denote the segments shown in Fig. 9. The red dashed line corresponds to the boundary between the main body of the rock avalanche and the carapace. Drone photo N. Akçar

as "Toma 658." In the overall view in Fig. 10E, one recognizes a nearly vertical contact between the Tamins rock avalanche deposit and the Bonaduz formation. Elsewhere, the Bonaduz formation rests in more or less horizontal contact on top of the Tamins rock avalanche deposits, underlining its younger age. The steep contact at Tuma dil Bregl points to a dynamic contact. Calhoun and Clague (2018) attributed the rock avalanche deposit to the Flims rock avalanche and explained the steep contact as resulting from a forced emplacement and shearing. Detailed mapping of the area however suggests that the rock avalanche deposit pertains to the Tamins rock avalanche, which in this area (just across the Hinterrhein river) is composed of Permian volcanics (Plattazüg formation). These volcanics are unequivocally derived from the source area of the Tamins rock avalanche. This provides further evidence that the (younger) Bonaduz formation was mobilized by the impact of the Flims rock avalanche and intruded and entrained the Tamins rock avalanche deposit. Figure 10F depicts the top of the Tamins rock avalanche deposit in which angular ill-fitting blocks of Quinten limestone lie on top of smaller fragments interspersed with larger angular blocks, a situation that is reminiscent of a carapace.

Pre-failure topography and failure of the rock avalanche

To assess the pre-event topography of the source area, the contour lines of the slopes east and west of the lateral scarps were extrapolated and linked (Fig. 11). Two features needed to be included. First, the gorge east of the source area was extended southward. This gorge was cut into highly fractured rocks along the Kunkelspass fault zone exposed in a tunnel south of Kunkelspass (Pfiffner and Wyss in press). Within the gorge, mapping revealed the existence of horizontally layered Pleistocene conglomerates and sands, which predate the Tamins rock avalanche event. Second, a ridge reaching more than 2000 m a.s.l., which extended from Säsagit to the SE, is postulated. This ridge is needed to explain the dry gullies east of Säsagit, which end blindly above the head scarp (Fig. 1). Considering the 3D geometry of the Glarus thrust, one could expect a klippe of Permian clastics or volcanics once existed on the SE tip of this ridge.

A further feature of the pre-event structure of the rock avalanche is the basal detachment or gliding surface and the base of the deposit in the accumulation area. The basal detachment surface can be assessed in the zone of depletion where a thin veneer of rock avalanche deposit (if at all) overlies the bedrock. The base of the deposit can be estimated from the glacial to post-glacial fill of the over-deepened valley. As discussed above, it is reasonable to assume that the valley floor prior to the Tamins event was at around 500 m a.s.l. Based on these arguments, the failure surface and the base were reconstructed and presented with contour lines as shown in Fig. 12. In the zone of depletion, the surface is constrained by the lateral scarp. In the accumulation zone, it must be assumed that the overdeepened Rhine valley extended upvalley along the Vorderrhein and the Hinterrhein and that gravity spreading of the rock avalanche deposit occurred as indicated by the present-day shape of its outer limit.

Based on the map in Fig. 12, a cross-section was constructed and is shown in Fig. 13. Nearly isoclinal folds dominate the bedrock geology. These folds formed while the rocks were still buried deep in the subsurface at temperatures exceeding 300 °C (Pfiffner, 2011) and are accompanied by a penetrative foliation. In limestone, this foliation is an expression of a shape-preferred orientation of calcite grains underlined by (scarce) sheet silicates aligned parallel to the long axes of the calcite grains. The resulting anisotropy is responsible for a rock cleavage, which is subparallel to the basal rupture surface of the rock avalanche (see Fig. 13). The foliation may thus have acted as a plane of weakness for the development of the basal rupture and sliding surface. The pre-event topography indicated in the cross-section of Fig. 13 was taken from Fig. 11. Noteworthy is a break in slope at the foot of the paleo-valley flank.

The paleo-klippe of Glarus nappe SE of Grossalp very likely consisted of Permian Verrucano, which locally contains volcanics

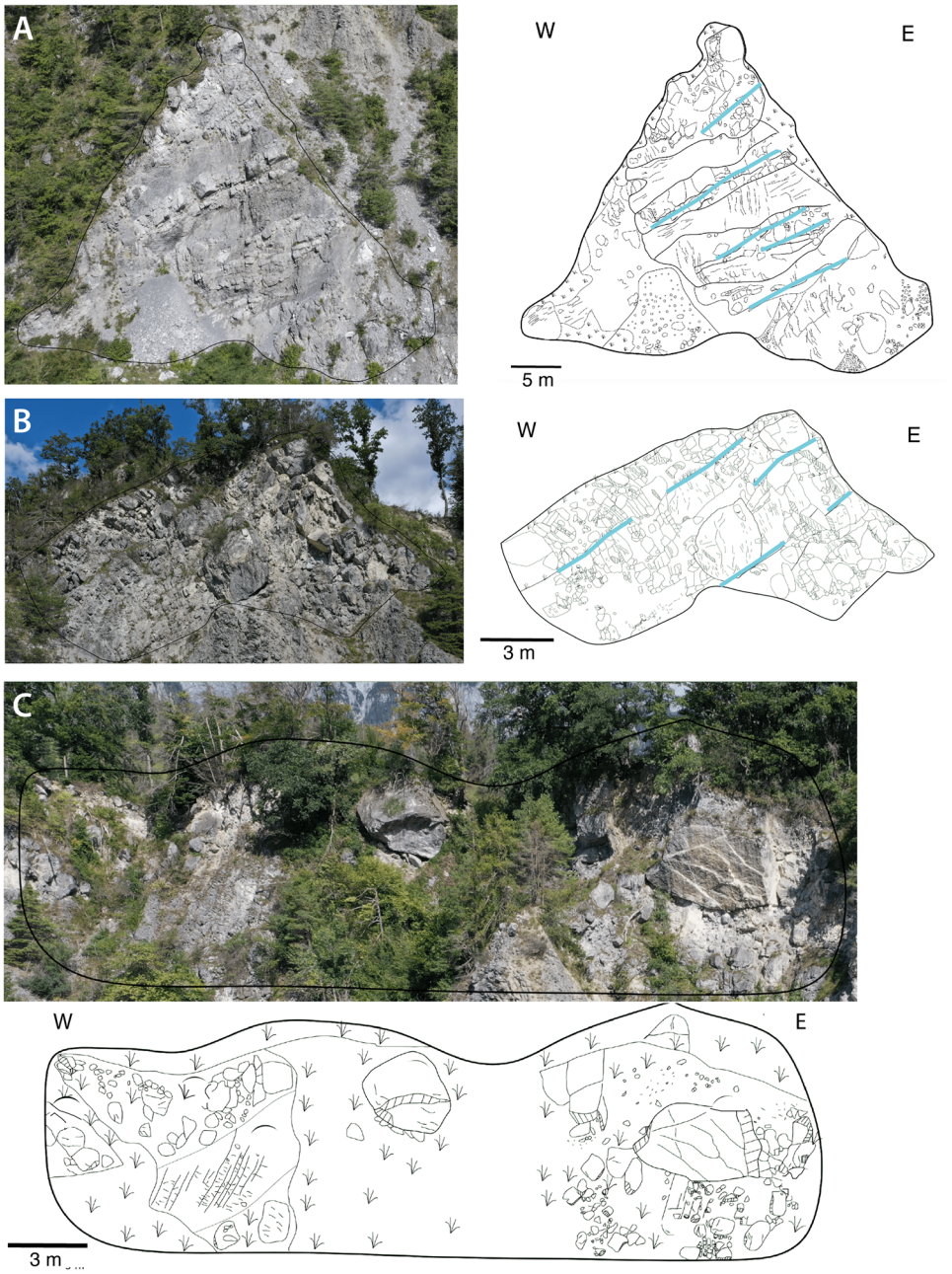

Fig. 9 Detailed views of outcrop Fanaus. **A** Large fractured limestone block with preserved bedding structures. Bedding is easily observable and outlined by blue lines in the line diagram. **B** Blocky texture in fractured limestone. Bedding is less visible and outlined by blue lines in the line diagram. **C** Blocky texture in fractured limestone with large blocks surrounded by smaller blocks

comparable to the ones of the Plattazüg formation in the footwall of the Glarus thrust. Such a klippe would explain the occurrence of Permian volcanics on top of Rascheu in the Tamins rock avalanche. As pointed out by Pfiffner and Wyss (in press), it is quite impossible to conceive an origin from the side scarps. The geometry at the base of the rock avalanche is drawn as a somewhat irregular line for some entrainment or bulldozing. However, the exact geometry of the units, including the contact between the (glacio-) lacustrine sediments and the gravel above it, remains speculative. The internal structure of the rock avalanche is shown to have two extensional scarps, which continue at depth as normal faults witnessing extension at the trailing edge of the rock avalanche upon slowing down of the moving mass. Between Cartschitscha and Tuma da Zislis in Fig. 13, two breaches are shown. The wider one was caused by the impingement that followed the impact of the Flims rock avalanche, and the narrow and deeper one represents sub-recent incision of the Rhine River, which can be followed further down the Rhine Valley.

In the cross-section, the failure surface cuts across the fold structure in the bedrock but is sub-parallel to the axial-planar cleavage (foliation). There was no single weak layer available as décollement horizon. But as noted above, the cleavage could have played a role in the development of the failure surface. The steep paleo-slope together with the abrupt change in slope at its base

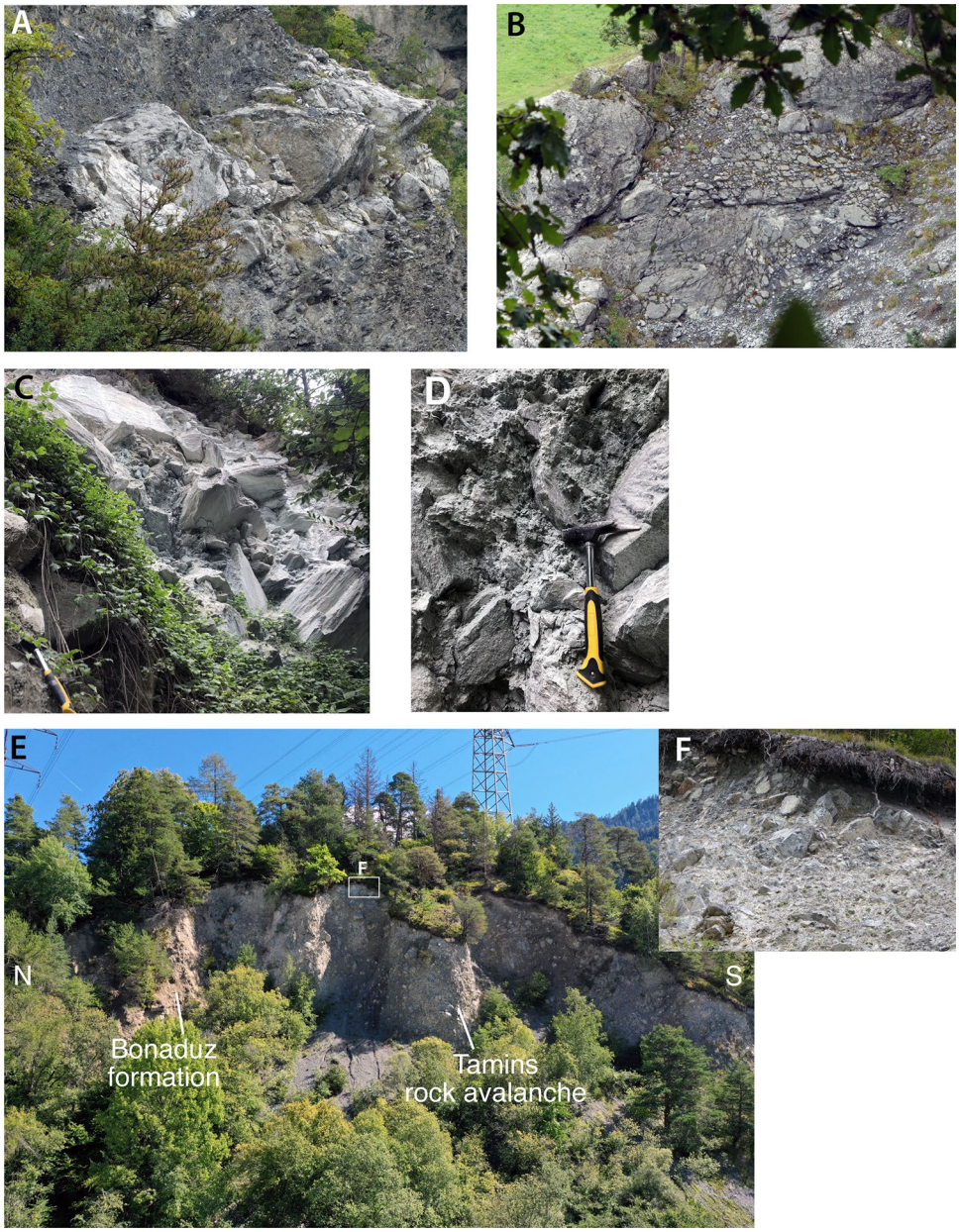

Fig. 10 Close-up views of rock avalanche deposits at Fanaus. **A** Bedding preserved within a massive limestone layer. **B** Jigsaw structure in fragmented limestone. Photographs O. Steinemann. **C** View of carapace in a former quarry at Plong Leula showing tilted blocks (Permian volcanics of Plattazüg formation). **D** Crushed fragments between larger blocks. Photographs S. Ivy-Ochs. **E** Outcrop on an erosional scarp of the Hinterrhein at Tuma dil Bregl; note near vertical contact between rock avalanche deposit and Bonaduz formation. **F** Detailed view of carapace (Quinten limestone). Photographs O. Steinemann

points to a gravitational instability that may have torn down the rock avalanche.

Combining the orientation and extent of the basal failure surface with the paleo-topography on the one hand, and the base of the rock avalanche deposits in the accumulation zone with the current topography (including a restoration of the Reichenau breach) on the other, the volume of the rock avalanche was calculated to 1.2, respectively 1.4 km^3. The 14% increase in volume due to fragmentation is less than the 25% estimated by Hungr and Evans (2004) for other rock avalanches based on the porosity of 18–35% of loosely placed crushed material reported by Sherard et al. (1963).

In a next step, a kinematic model was developed which shows the evolution of the Tamins rock avalanche in three time frames (see Fig. 14). The pre-failure situation is derived from along-strike projection (Fig. 14A) of regional structures. The post-failure structure shown in Fig. 13C reflects the mapped distribution of the lithologies within the rock avalanche. A large fold with inverted limb characterizes the pre-failure situation. During emplacement, the rock avalanche underwent a simple shear deformation with the top moving faster than the base, which resulted in a rotation of the fold limb (Fig. 14B). As the rock avalanche spread across the valley, the trailing edge moved slower and thus underwent extension as witnessed by the extensional scarps south of Rascheu and Cartschitscha. The geometry shown in Fig. 14C corresponds to the situation prior to the Reichenau breach induced by the Flims rock avalanche.

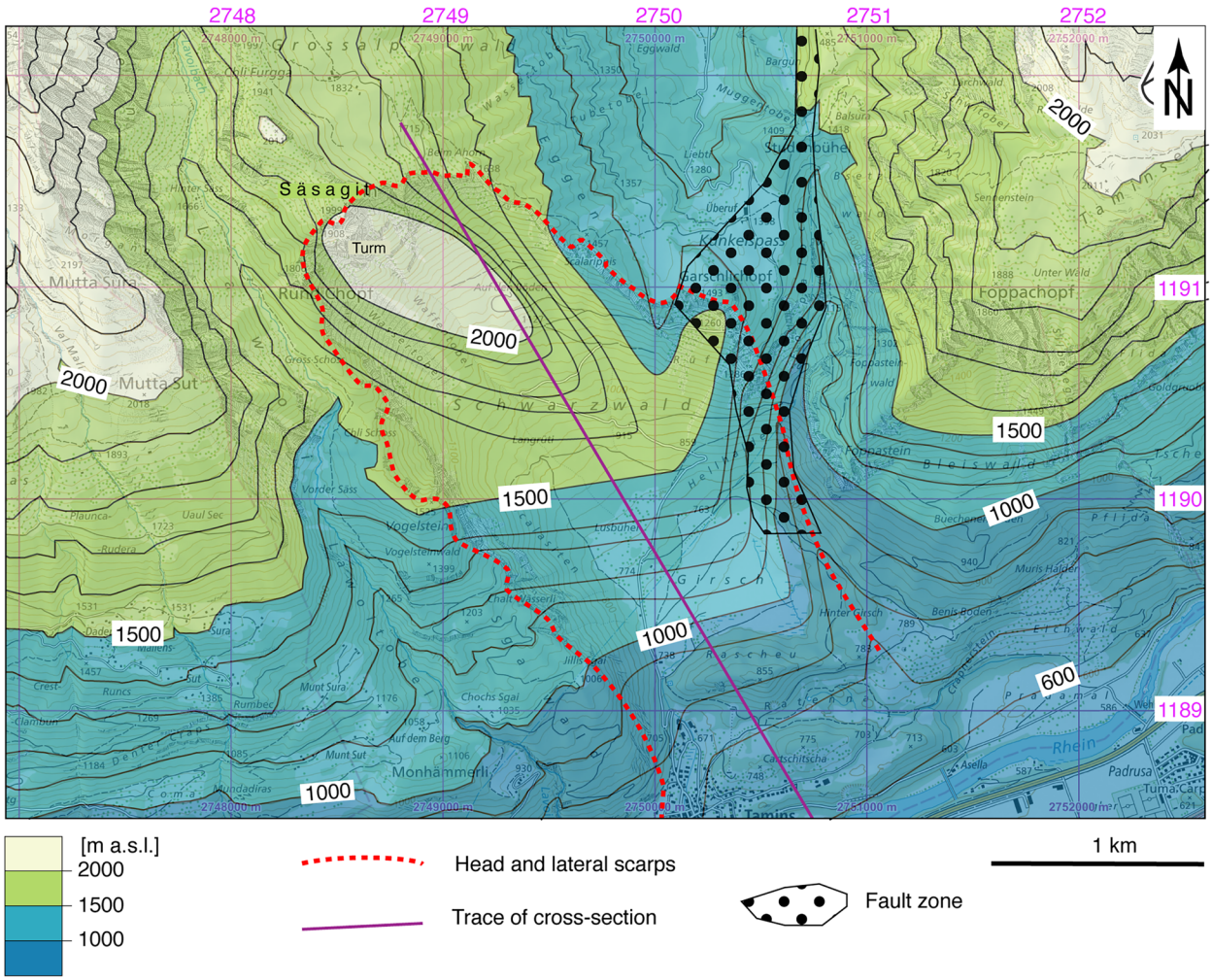

Fig. 11 Pre-event topography of the source area of the Tamins rock avalanche shown as contour lines

Cosmogenic ^{36}Cl exposure dating

Cosmogenic nuclides build up within rock surfaces exposed to cosmic rays. Determination of their concentrations allows calculation of how much time has elapsed since beginning of exposure and in the case of rock avalanche boulders since the rock slope failure event (Ivy-Ochs et al. 2017). To determine the age of the Tamins deposits, we took samples from the tops of eight large boulders (> 2 m high) located all across the Tamins rock avalanche deposits (Fig. 15A–F). Samples Tamins 50–53 and 55–57 are Quinten limestone boulders, while Tamins 54 is a boulder of prasinite (volcanics of the Permian Plattazüg fm) (Table 1). The top few centimeters (1–4 cm) were sampled using a hammer and chisel or a battery-operated saw.

Sample preparation for accelerator mass spectrometry (AMS) measurements followed Ivy-Ochs et al. (2004) implementing isotope dilution. Rock samples were crushed and sieved to <0.4 mm, and then leached in a weak HNO_3 solution. After addition of ~3.5 mg of ^{35}Cl carrier, 65–70 g of each sample was dissolved completely using HNO_3. For the one silicate rock sample (Tamins 54), a combination of HF and HNO3 was required to dissolve the rock. AgCl was precipitated by adding $AgNO_3$. To remove the isobar ^{36}S, $BaSO_4$ was precipitated by addition of $Ba(NO_3)_2$. The final AgCl precipitate was dried and pressed into tantalum targets for AMS measurements.

^{36}Cl and stable Cl measurements were done at the Laboratory of Ion Beam Physics, ETH Zurich, with the 6 MV tandem accelerator (Synal et al. 1997; Christl et al. 2013; Vockenhuber et al. 2019). Sample and blank ratios were measured against the standard material K382/4 N with a value of $36Cl/Cl=17.36 \times 10^{-12}$ (Vockenhuber et al. 2019). Blank values applied are $2.0 \pm 0.7 \times 10^{-15}$ for samples Tamins 50–53 and 55–57 and $3.3 \pm 0.4 \times 10^{-15}$ for Tamins 54. The chemical composition of every sample analyzed for ^{36}Cl was determined on aliquots by Actlabs, Ontario, Canada (Table 2).

^{36}Cl exposure ages were calculated with an in-house MATLAB code developed at Ion Beam Physics, ETH Zurich. All production rates and calculation parameters are given in Alfimov and Ivy-Ochs (2009). Implemented spallation production rates at sea level

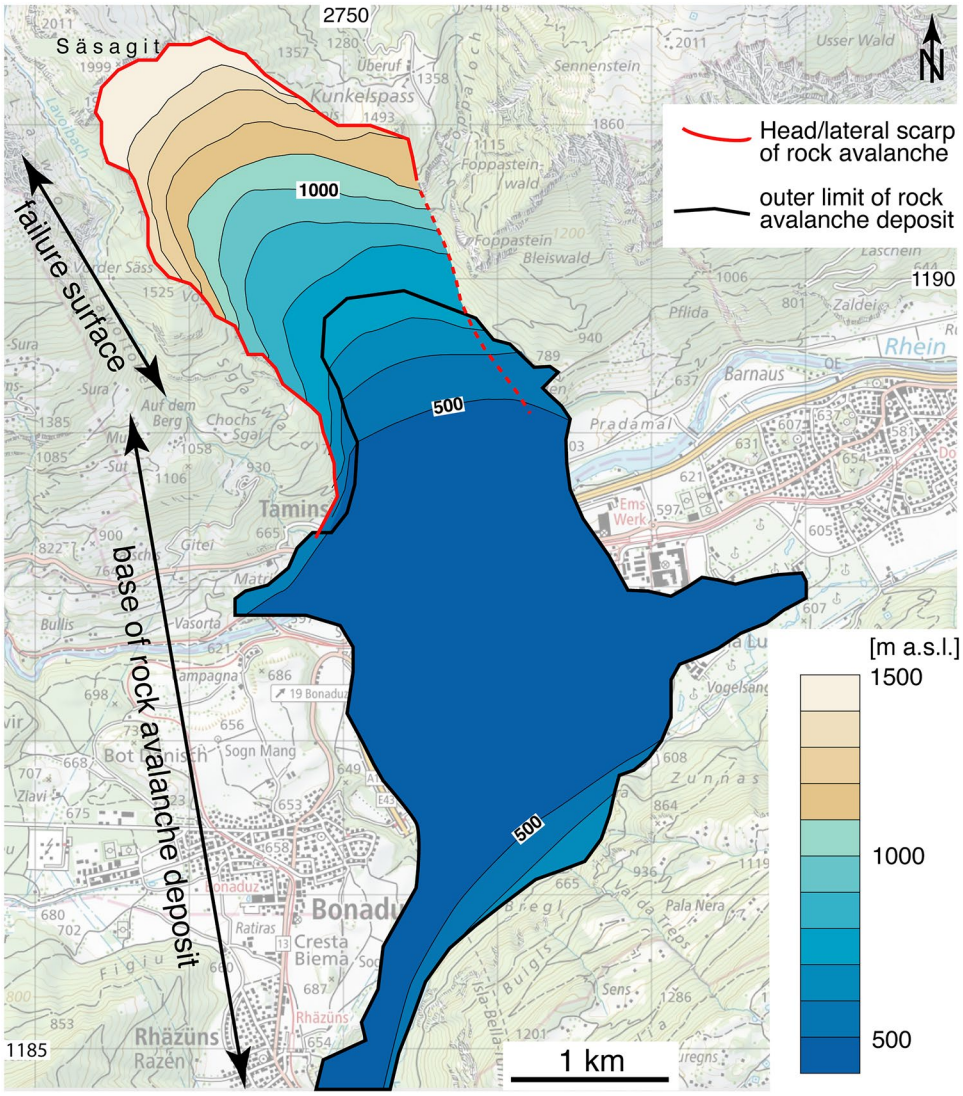

Fig. 12 Failure surface and base of the Tamins rock avalanche shown as contour lines

and high latitude are 48.8 ± 3.4 at/g_{Ca}/a for Ca (Stone et al. 1998) and 162 ± 24 at/g_K/a for K (Evans et al. 1997). These values agree well with recently published production rates (Borchers et al. 2016; Marrero et al. 2016). All data required for the calculations are given in Tables 2 and 3. Final age uncertainties (1σ) include both AMS uncertainties and the propagation of input uncertainties, including those of the production rates and their scaling.

An erosion-correction to an exposure age is required, especially for limestone surfaces. A range of values have been reported for limestone surface weathering rates (Plan, 2005; Häuselmann 2008; Krklec et al. 2018). Häuselmann (2008) measured a karst weathering rate of 14 ± 7 mm/ka in Schrattenkalk limestones in central Switzerland. For limestone bedrock surfaces in Slovenia, Krklec et al. (2018) determined rates of 21.5 ± 1.3 mm/ka. We use here an erosion rate of 10 mm/ka to correct the ^{36}Cl exposure ages of Quinten limestone boulders (Tamins 50–53, 55–57). The one silicate boulder analyzed, Tamins 54 (Plattazüg volcanics), was corrected for erosion using a rate of 1 mm/ka (André 2002). Both corrected and uncorrected ages are given in Table 3, and corrected ages are shown in the map of Fig. 16.

Modeling

3D runout modeling of the Tamins rock avalanche was performed in order to place the mobility of this event into a wider context, to verify a single volume failure scenario, and to provide further evidence for the geomorphological interpretation. The numerical model Dan3D (McDougall and Hungr 2004) was used, modified to account for the initial coherence exhibited by many rock avalanches (Aaron and Hungr 2016). The combined model, Dan3D-Flex, initially treats the mass as a flexible block, which rotates and translates over the input topography. At a user-specified time, the program switches to the original Dan3D algorithm, which is a depth-averaged Lagrangian model that solves the equations of motion using Smooth Particle Hydrodynamics, and simulates the rock avalanche as a frictional fluid whose behavior is governed by internal and basal rheologies. A detailed description of the rheological models available in Dan3D-Flex is provided in Hungr and McDougall (2009). Two rheologies, the frictional and Voellmy, are used in the present work. The frictional rheology features one calibrated value, the bulk friction angle, and is appropriate for simulating the initial

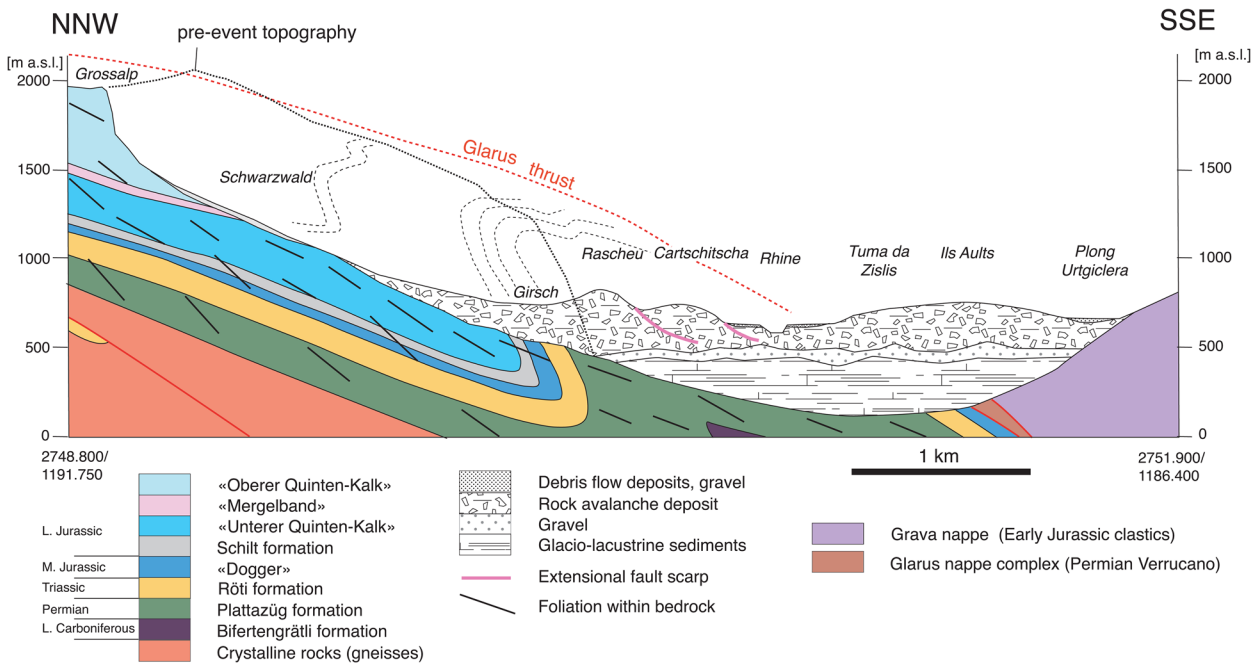

Fig. 13 Cross-section through the Tamins rock avalanche. Trace is given in Fig. 11

stages of rock avalanche motion, when the failed mass is moving over the basal rupture surface. The Voellmy rheology features two calibrated parameters, a friction coefficient and turbulence coefficient, and is appropriate for simulating rock avalanche interaction with path material (Aaron and McDougall 2019).

As input, Dan3D-Flex requires three topography files: (1) the thickness and location of the source mass, (2) a topographic file representing the surface that the rock avalanche moved over, and (3) the locations of any material changes. Additionally, relevant material properties must be input into the model. The first two topography files were obtained based on the surface reconstruction described in the "Pre-failure topography and failure of the rock avalanche" section, and the third topography file, as well as the material properties, is described below.

The runout simulations of the Tamins rock avalanche were parameterized based on the methodology used by Aaron and McDougall (2019). For this, two rheologies were used, a frictional rheology in the source zone and a Voellmy rheology along the path, with the location of the material change shown on Fig. 16A. This model parameterization is useful to separately analyze the basal resistance acting in the source zone from that acting along the path, where the material may override and entrain path material (e.g., Aaron and McDougall 2019). As all other parameters were fixed, three parameters for the two material simulations were calibrated. Preliminary testing indicated that a friction angle of 10° is required for the failed material to vacate the source zone, so this parameter was fixed at this value for the calibration. The Voellmy friction and turbulence coefficients were then calibrated using a posterior analysis (Aaron and McDougall 2019), with friction coefficients ranging from 0.25 to 0.4 and turbulence coefficients ranging from 100 to 2000.

The runout modeling results are in concert with the hypothesized failure scenario, as well as the geomorphic interpretation. The best-fit final deposit depths and maximum velocities for the runout models are shown on Fig. 16B, and timelapse results are shown on Fig. 17. The best-fit parameters obtained are summarized in Table 4. Starting with Fig. 16A, B, it can be seen that the overall impact area of the rock avalanche is reasonably well produced by the simulation, although the eastern extent of the deposit is overpredicted. This could either be due to excessive spreading predicted by the model, or reworking of the deposit following the emplacement of the adjacent Flims rock avalanche, which triggered a massive hyperconcentrated flow (e.g., Calhoun and Clague 2018). Deposit thicknesses in the valley are greater than 200 m in certain areas, which matches our pre-failure reconstruction of the topography, and maximum velocities reach about 55 m/s, with an average value of around 35 m/s. It was impossible to simulate the distal south-western extent of the debris, as both this distal tongue and the observed narrow width of the deposit could not be reproduced simultaneously. This could potentially indicate that different substrate conditions existed at the distal end of the debris, although at present direct evidence for this is lacking, or that a portion of this distal end was later removed, entrained by the Flims rock avalanche and the associated hyperconcentrated flow; Tamins rock avalanche pieces were carried southward way up along the Hinterrhein (Remenyik 1959).

The timelapse simulation results shown on Fig. 17 suggest that the Tamins rock avalanche likely travelled for a significant distance as a flexible block, before fragmenting and turning flowlike (this was specified to occur at 80 s). This was required in our simulations in order to simultaneously reproduce the thick deposit in the valley floor and the narrow impact area. A long rigid motion distance

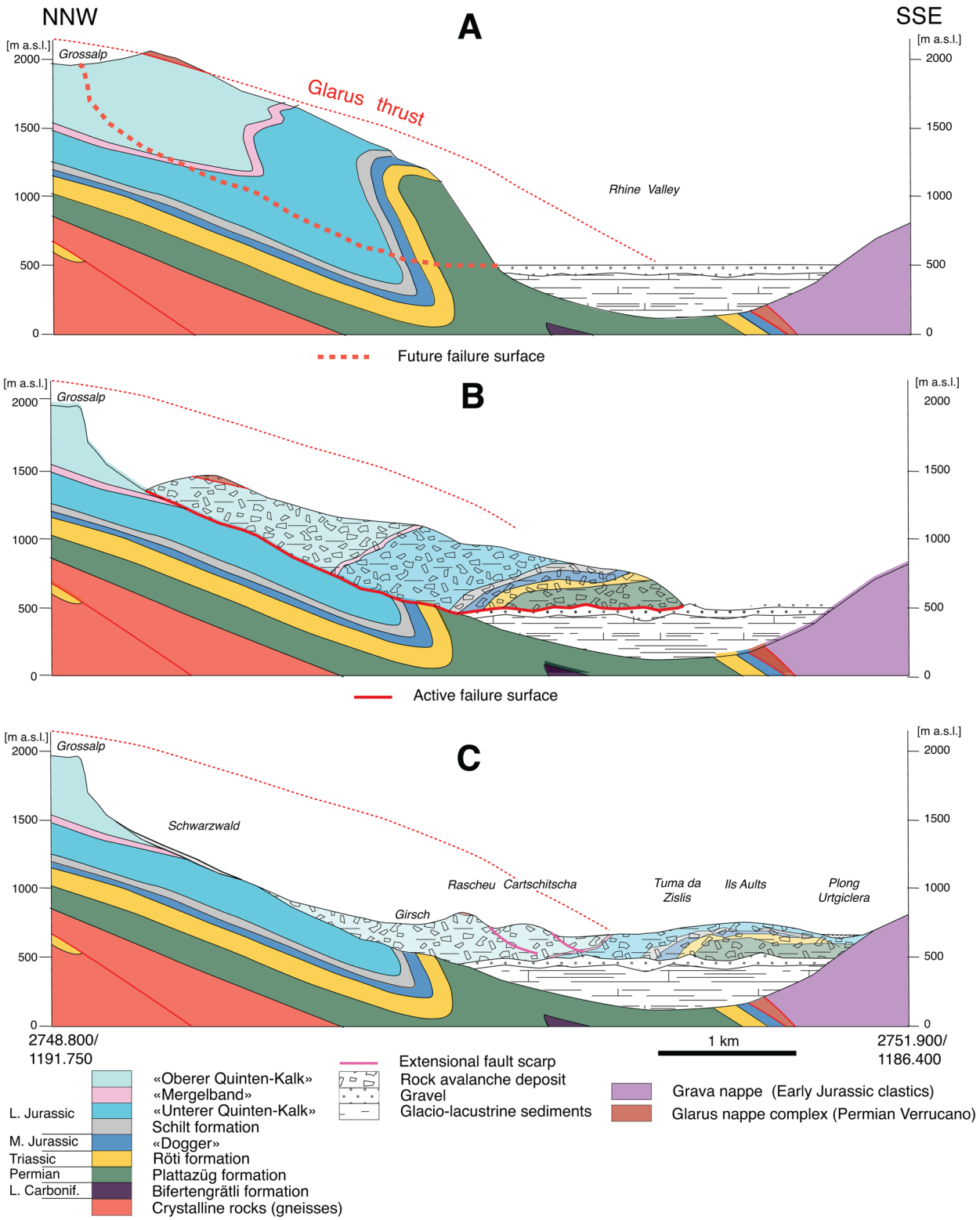

Fig. 14 Kinematic model of the Tamins rock avalanche. **A** Pre-failure situation. **B** The rock avalanche has broken away; shearing has rotated the lithologic units at the front of the rock avalanche. **C** The rock avalanche has settled; situation pre-Reichenau breach

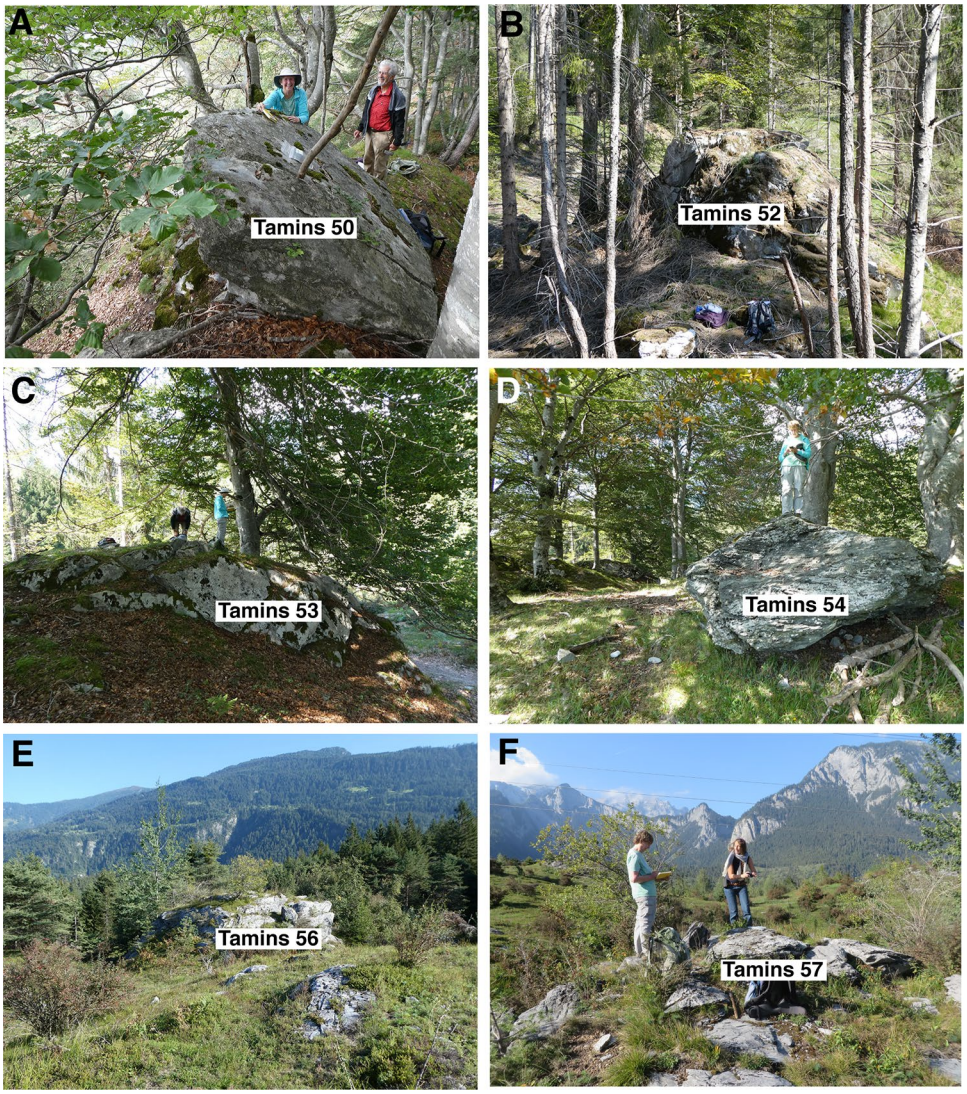

Fig. 15 Sampled boulders. Photographs by authors

Table 1 Samples and sample locations (Swiss National km grid coordinates LV95)

Sample	EW coord.	NS coord.	Lithologic unit
Tamins 50	2750.475	1189.155	Quinten limestone
Tamins 51	2750.705	1189.260	Quinten limestone
Tamins 52	2750.955	1189.280	Quinten limestone
Tamins 53	2751.000	1189.330	Quinten limestone
Tamins 54	2751.040	1189.385	Prasinite
Tamins 55	2751.160	1187.415	Quinten limestone
Tamins 56	2751.270	1187.670	Quinten limestone
Tamins 57	2751.235	1187.730	Quinten limestone

was also noted in simulations of the adjacent Flims rock avalanche (Aaron et al. 2020). Our simulations show that the mass impacted the valley floor after about 40 s, and the mass spread both to the southeast and southwest following fluidization. Thick deposits at Rascheu are apparent in the simulation, which reasonably reproduce field observations.

Discussion

Geomorphology and age of the Tamins rock avalanche

Deposit morphology of rock avalanches are widely used to derive flow patterns (Barth 2013; Zeng et al. 2019; Chen et al. 2022). These include lateral, transverse, and longitudinal ridges, hummocks, closed basins, and extensional scarps. Longitudinal ridges are a prominent feature of rock avalanches. According to Dufresne and Davies (2009), these ridges (and associated features) form parallel to the flow direction and are interpreted to be a result of intrinsic processes of granular flows with a free surface. Ils Aults is a longitudinal ridge and quite obviously parallel to the flow direction. At the

Table 2 Samples with major and trace element concentrations

Sample	Al_2O_3 (%)	CaO (%)	Fe_2O_3 (%)	K_2O (%)	MgO (%)	MnO (%)	Na_2O (%)	P_2O_5 (%)	SiO_2 (%)	TiO_2 (ppm)	Sm (ppm)	Gd (ppm)	U (ppm)	Th (ppm)	Cl* (ppm)
Tamins 50	0.35	47.78	0.18	0.11	5.60	0.006	0.03	0.05	0.90	0.014	0.4	0.4	1.1	0.6	11.48 ± 0.10
Tamins 51	0.17	51.53	0.09	0.04	3.11	0.007	0.02	0.04	0.58	0.006	0.3	0.3	0.7	0.2	11.80 ± 0.07
Tamins 52	0.17	54.06	0.08	0.04	1.01	0.005	0.03	0.04	0.47	0.005	0.3	0.3	0.6	0.4	1.71 ± 0.06
Tamins 53	0.18	53.78	0.10	0.04	1.07	0.006	0.02	0.04	0.47	0.007	0.3	0.3	0.6	0.3	4.13 ± 0.07
Tamins 54	12.96	16.12	7.12	0.11	3.61	0.167	4.48	0.22	41.88	0.970	5.9	4.7	2.5	5.8	8.16 ± 0.38
Tamins 55	0.40	54.24	0.19	0.10	0.66	0.020	0.03	0.07	0.88	0.014	1.2	1.3	0.2	0.4	1.12 ± 0.11
Tamins 56	0.17	54.71	0.11	0.04	0.92	0.019	0.03	0.06	0.45	0.006	0.8	1.0	0.3	0.4	2.58 ± 0.09
Tamins 57	0.18	53.02	0.10	0.04	1.68	0.014	0.03	0.07	0.69	0.005	0.6	0.8	0.2	0.4	2.59 ± 0.14

*AMS measured

trailing edge of the rock avalanche mass, transverse ridges truncate the longitudinal ridge. We interpret that these transverse ridges are the result of extension in the flow direction as the trailing part of the flowing mass slowed down.

At the leading edge of the mass, diversion of flow to the east and west occurred, whereas no runup to speak of can be observed on the opposing mountain flank. An erosional removal of a potential runup is highly unlikely. The deflection is interpreted as a consequence of high mobility and gravity spreading. The eastward deflection was accompanied by several east-dipping normal faults which produced N-S oriented elongate hills aligned behind each other. The low friction on the water saturated substrate inhibited bulldozing, which is also indicated by the lack of signs of substrate being entrained or mobilized. The westward deflection is more difficult to assess because this area was strongly overprinted by the impact of the Flims rock avalanche and the associated mobilization of the substrate, i.e., the Bonaduz formation. The overprint resulted in moving blocks of the Tamins rock avalanche deposit southward up the Hinterrhein for several kilometers. Bulldozing is indicated by steep contacts between rock avalanche deposits and Bonaduz formation (see Fig. 9E).

As Davies and McSaveney (2009, 2012) argue, fragmentation of the moving body of rock avalanches plays a major role in their flow behavior. The interior of the Tamins rock avalanche is, apart from the carapace, unfortunately only marginally exposed. In the outcrop at Fanaus, the internal structure of the top part of the rock avalanche body displays a jigsaw pattern and contains many larger blocks in some of which original bedding is preserved (Fig. 8). Given the observations of Pfiffner and Wyss (in press) and Pfiffner (2022) in the neighboring Flims rock avalanche, fragmentation in the Tamins rock avalanche seems minor in comparison, but cannot be ruled out in the lower, still hidden part of the main body.

One of the major questions addressed in this work is the age of the Tamins rock avalanche and its relationship to the neighboring Flims rock avalanche. The Bonaduz formation is the key to determine the relative chronology of events. Quite clearly this formation was deposited on top of the Tamins rock avalanche, as

Table 3 Samples with AMS data and ^{36}Cl exposure ages

Sample	Lithology	Longitude WGS84	Latitude	Elevation	Thickness	Topographic shielding	^{36}Cl	Exposure age No erosion	Exposure age 10 mm/ka
		DD.DDD	DD.DDD	m a.s.l	cm		10^6 atoms/g_{rock}	Years	Years
Tamins 50	QL	46.836	9.411	848	1	0.9769	0.343 ± 0.020	9200 ± 600	9700 ± 600
Tamins 51	QL	46.837	9.414	778	1.2	0.9783	0.304 ± 0.010	8000 ± 400	8400 ± 400
Tamins 52	QL	46.837	9.417	788	2	0.9701	0.326 ± 0.016	7500 ± 500	9100 ± 500
Tamins 53	QL	46.838	9.418	796	1.5	0.9827	0.341 ± 0.012	8700 ± 400	9200 ± 400
Tamins 54	PV	46.838	9.419	800	1.5	0.9799	0.118 ± 0.018	9200 ± 1400	*9300 ± 1500
Tamins 55	QL	46.821	9.419	712	1.5	0.9910	0.284 ± 0.031	7600 ± 900	8100 ± 900
Tamins 56	QL	46.823	9.421	710	1.5	0.9912	0.344 ± 0.016	9200 ± 500	9900 ± 600
Tamins 57	QL	46.823	9.421	718	2	0.9943	0.262 ± 0.013	7100 ± 400	7500 ± 400

QL Quinten limestone, PV Plattazüg volcanics (prasinite)

*Erosion rate of 1 mm ka^{-1}

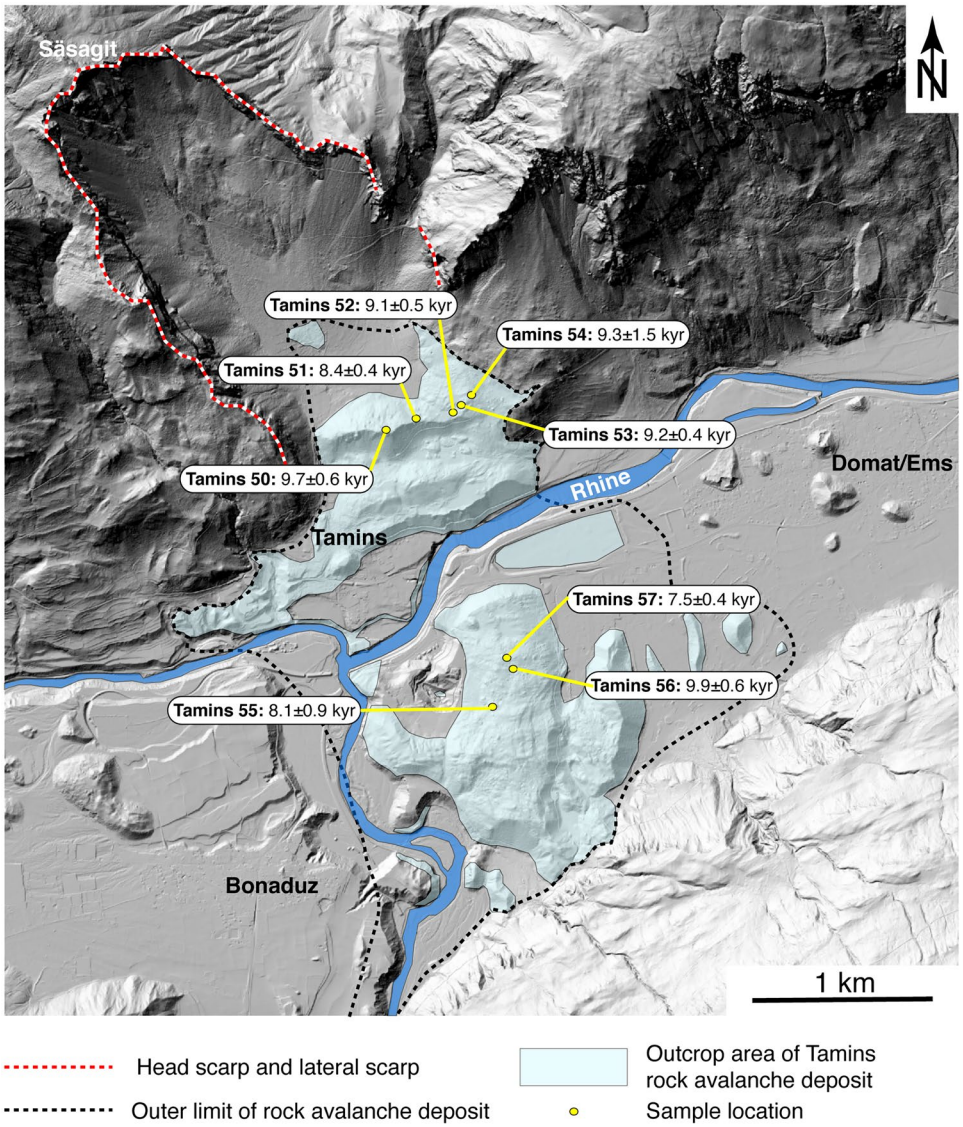

Fig. 16 Digital elevation model with boulder locations and ages

can be observed in numerous outcrops. On the other hand, the Bonaduz formation, which consists of massive gravel and sand transported as a hyperconcentrated flow (Calhoun and Clague 2018), was formed by the impact of the Flims rock avalanche into (paleo) lake Bonaduz. The mobilized substrate of the Flims rock avalanche impinged and overtopped the longitudinal ridge Ils Ault of the Tamins rock avalanche and breached it (Fig. 5). Thus, it is clear that the Tamins rock avalanche is older than the Flims rock avalanche. The material removed during breaching was transported downstream and deposited as isolated 100-m-sized hills, the so-called tumas. According to ERT sounding, the displaced rock avalanche deposits are up to 200 m thick (Knapp et al. 2022). In some instances (e.g., Tuma Casté), the tuma consists of Tamins rock avalanche fragments in vertical contact to silt deposits derived from the Bonaduz formation.

The stratigraphic relationships of the Bonaduz sediments provide a basis on which to scrutinize the obtained exposure ages. The erosion-corrected exposure ages of the Tamins boulders range from 7500 ± 400 years (Tamins 56) to 9900 ± 600 years (Tamins 57; see Table 4). The average of all obtained exposure ages is 8880 ± 1080 years. This uncertainty is based on the cumulative probability of uncertainties for every sample based on a Gaussian distribution (1σ). The standard deviation of the mean is 820 years. Exposure ages from landslide deposits can scatter, with both too old and too young ages being present (Martin et al. 2014). Interpretation of exposure ages requires conformity with independent field evidence and the calculation of a mean age from all data may not be justified in all cases, as has been discussed in detail for moraine dating (cf. Ivy-Ochs et al. 2007; Winkler 2018). The Bonaduz formation sediments, which overlie Tamins deposits, were deposited as a consequence of the Flims rock avalanche. This event occurred at 9475–9343 cal BP (Deplazes et al. 2007; radiocarbon data recalculated in Nicolussi et al. 2015). Three of our boulder ages are younger than and do not overlap with the age of the Flims event. These are Tamins 51 (8400 ± 400 years), Tamins 55 (8100 ± 900 years), and Tamins 57 (7500 ± 400 years). It is likely that the surfaces of these three boulders were affected by post-depositional processes, such as spalling (Tamins 51), or were covered by sediment for part of

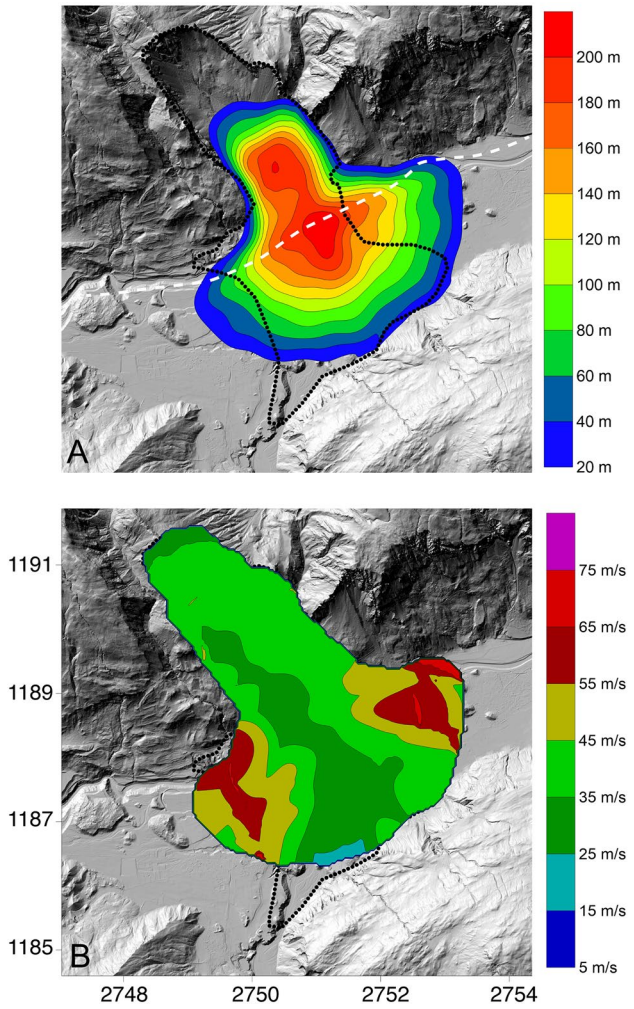

Fig. 17 **A** Best-fit deposit depths obtained with Dan3D-Flex. The dashed black outline shows the observed impact area, and the dashed white line shows the location of the material change from the frictional rheology to the Voellmy rheology. **B** Maximum simulated velocities at each impacted location

their exposure history (Tamins 55 and 57). The exposure ages of these three boulders are too young and do not reflect the time of deposition. The newly calculated average based on the remaining five ages is 9420 ± 880 years, with a standard deviation of 340 years. Field relationships and the exposure dating suggest that Tamins rock avalanche occurred as a single event just before the Flims rock avalanche.

Regarding the trigger, structural preconditioning by a pervasive joint system and the Kunkelspass fault zone has played a role (see discussion above). Krietsch and Wolter (2018) and Lemaire et al. (2020) also suggested as structureal preconditioning judging from bedding plane orientations. Apart from this, the break in slope of the pre-failure topography at 500 m a.s.l. (see Fig. 13) was likely responsible for high tensile stresses and may have controlled the position of the failure surface (Savage 1993; Wolters and Müller 2008). According to the Swiss Seismological Survey, the region around the Tamins rock avalanche has a more than average seismic activity within the Alps, and this area has a high uplift rate of 1.5 mm/a (Pfiffner 2014 and references therein). The area lies within a zone of post-glacial tectonic faults (Persaud and Pfiffner 2004). Thus, an earthquake shake might have been the ultimate cause to get the rock avalanche to move.

Table 4 Best-fit basal resistance values for the Tamins runout analysis

Friction angle (source zone)	10°
Friction coefficient (path)	0.32
Turbulence coefficient (path)	500 m/s^2

Repercussions of modeling

The runout analysis has revealed many interesting features regarding the emplacement of the Tamins rock avalanche, with implications for our geomorphic interpretation. As noted above on Fig. 17, the best-fit simulations require that the failed mass travelled as a coherent block for the majority of its motion. The present model is able to simulate either coherent block motion, or fully developed frictional flow. In reality, there is likely transitional behavior between these two; however, our simulation results indicate the Tamins rock avalanche was behaving closer to the coherent block end member. This is supported by the relatively small amount (14%) of bulking that occurred during this event (as evidenced by our pre-event surface reconstruction). Further, volume reconstructions of the Flims rock avalanche have also noted limited bulking (19% after Pfiffner 2022), and runout analyses required long rigid motion distances (Aaron et al. 2020). It thus appears as though these two rock avalanches, which both have anomalously high volume, do not bulk as much as other, mostly smaller, events. Further analyses of large (> 1 km^3) events are required to generalize this observation further.

Aaron and McDougall (2019) analyzed the phenomenon of long runout of rock avalanches considering variable substrates, namely bedrock, saturated and unsaturated substrate, and ice and snow. They concluded that the type of substrate strongly influences the rock avalanche mobility. The data points for bedrock and saturated and unsaturated substrate are shown in Fig. 18, along with the data point for the Tamins rock avalanche. The latter has a H/L ratio of 0.23 and plots beneath the data for bedrock and unsaturated substrate, supporting the interpretation that the substrate was saturated during the emplacement of the Tamins rock avalanche.

The best-fit back-analyzed parameters (Table 4) indicate that the mass experienced low resistance in the source zone, but relatively high resistance along the path. The path material values are at the upper range of those analyzed by Aaron and McDougall (2019), and the Voellmy friction coefficient analyzed for Tamins is a slightly more than double that analyzed for Flims (Aaron et al. 2020). Even given these high basal resistance values, the simulated deposit exceeds the mapped deposit extent in the northeast (Fig. 19). This location corresponds to where the Rhine river breached the Tamins deposit, which could potentially have eroded this debris. This observation, combined with the noted difference between calibrated friction coefficients for Flims and Tamins, provides further evidence that the Tamins

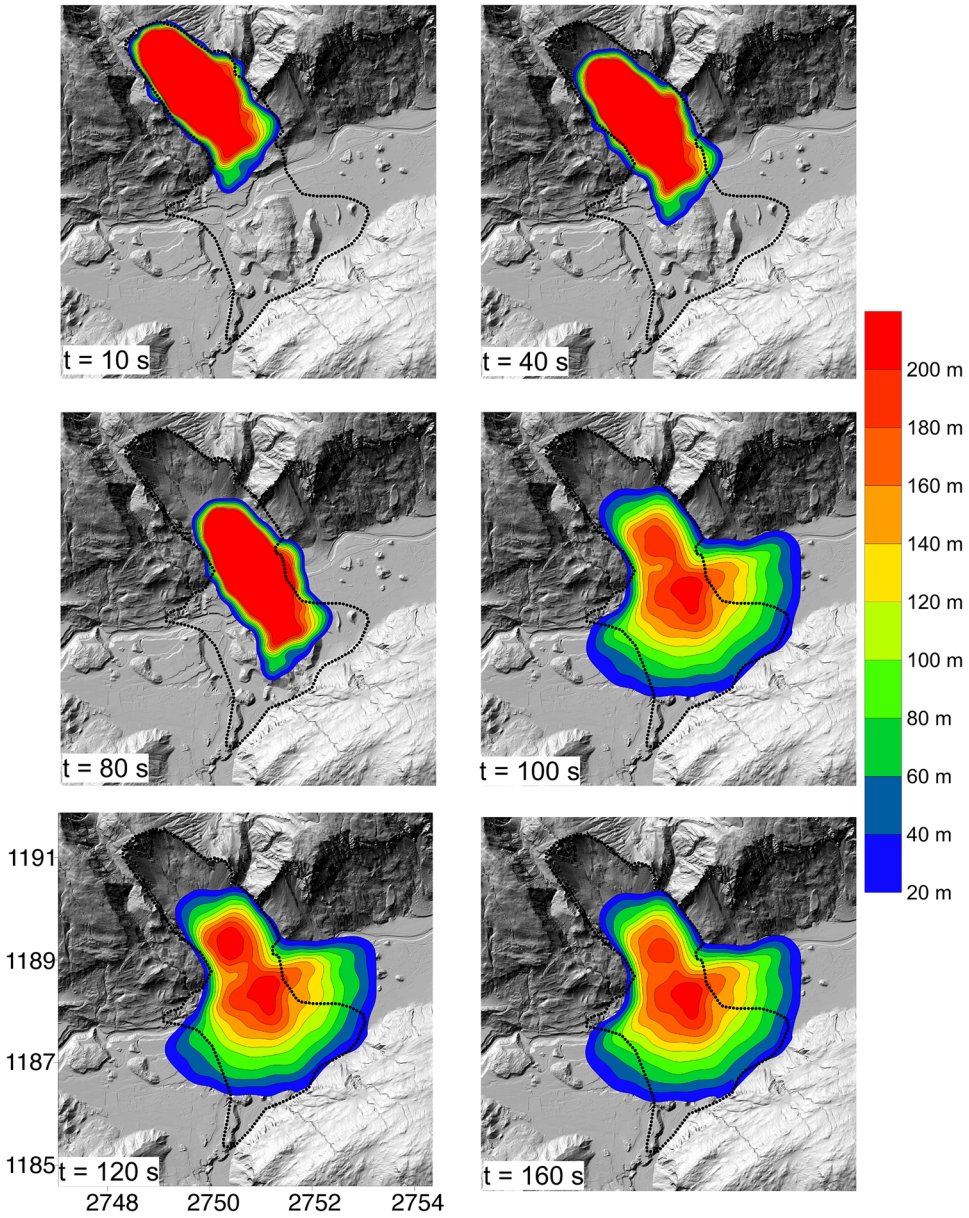

Fig. 18 Simulated deposit depths at different timelapse using the best-fit paramters

event pre-dated the Flims event, and dammed the valley to create Lake Bonaduz. This is because the coefficients indicate the path material was different for the two events, with Flims encountering a much weaker path material (highly saturated sediments beneath the lake), vs. Tamins where the path material may have been somewhat drier and less susceptible to rapid undrained loading. This is further supported by the measured H/L of this event, where, as mentioned above, the Tamins rock avalanche with a value of 0.23 plots slightly below bedrock and unsaturated substrate and is higher than the value of 0.18 obtained for the Flims rock avalanche (Pfiffner 2022).

One puzzling observation of our model results is the low friction angles back-analyzed in the source zone. Catastrophic failure of this event requires ultimate friction angles of 10°; however, no obvious weak horizons are noted in the source zone stratigraphy. As discussed above in conjunction with Fig. 13, an Alpine foliation parallel to the axial surface of the folds is observed in the rocks around the breakaway zone of the rock avalanche. This anisotropy may have played a role in the development of the sliding surface. In addition, a break in slope is to be expected at the foot of the mountain flank as shown in the pre-failure situation in Fig. 14A. According to Savage (1993) and Wolters and Müller (2008), such breaks result in high differential stresses and may control the structural position of the sliding surface.

Conclusions

Combining detailed field survey, sediment and landform analysis, cosmogenic nuclide surface exposure dating, and runout modeling allows to reconstruct the timing and dynamics of the Tamins rock avalanche. The Tamins rock avalanche deposits are located just a few kilometers downstream of the Flims rock avalanche deposits.

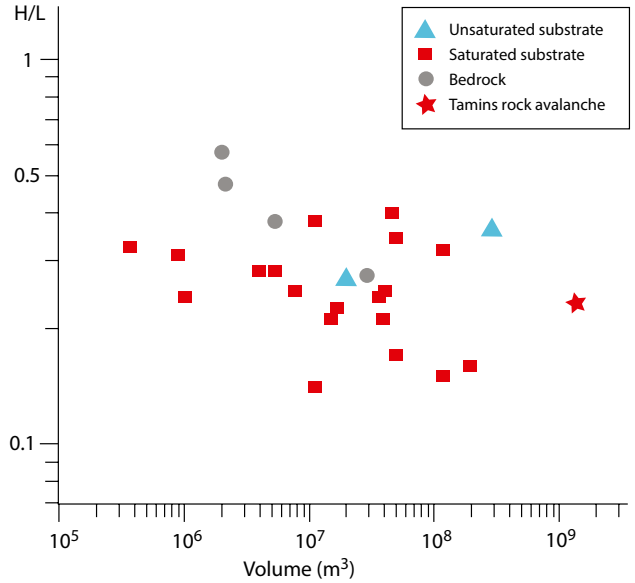

Fig. 19 H/L ratio versus volume of rock avalanches. Data from Aaron and McDougall (2019) complemented with the Tamins rock avalanche data

Although its volume (1.2 km^3) is notably smaller than that of the Flims event (11.5 km^3), its impact on the landscape was profound and enhanced by the Flims event.

The release area of the Tamins event lies in the horseshoe-shaped niche just below the peak Säsagit. The morphology of the deposits suggests that the Tamins rock avalanche broke away as a semicoherent block, which subsequently was sheared with a more slowly moving base. 3D runout modeling suggests incipient block movement followed by flowlike behavior. This modeling further suggests that the Tamins rock avalanche experienced relatively high basal resistance along the path, but that the strength in the source zone must have been low for catastrophic failure to occur. However, no weak basal layer which could act as failure surface has been identified, and the low frictional angle of 10° points to a different inherent weakness. The pervasive Alpine foliation within the rocks is a possible reason. Spreading of the rock avalanche body resulted in extensional scarps that separate large (1–2 km long) W-E trending transverse ridges (Rascheu, Carschitscha) in the northern more proximal sector. In contrast, in the south, in the distal displaced mass, longitudinal ridges (N-S trending) dominate (Ils Aults). Upon impacting the opposite Rhine Valley flank flow was deflected; east-directed gravity spreading is indicated by longitudinal ridges (Crest'Aulta, Tuma Lunga) associated with extensional scarps.

Exposure dating eight boulders located all across the Tamins rock avalanche deposits yields an age of the Tamins rock avalanche of 9420 ± 880 years BP which is close to but slightly older than the age of the neighboring Flims rock avalanche. The stratigraphic evidence showed that the Tamins event pre-dated the Flims event, but it was not known by how much. The ages as well as the morphology and internal structure of the Tamins rock avalanche suggest that it occurred as a single event.

Acknowledgements

The project emanated from a mapping project funded by the Geological Survey of Switzerland/swisstopo. The Laboratory of Ion Beam Physics headed by Professor Dr. Arno Synal is sincerely thanked for support of fieldwork, laboratory work, and accelerator mass spectrometry measurements. Thoughtful comments from two anonymous reviewers greatly improved the manuscript.

Author contribution

Conceptualization: OAP, SIO; methodology: SIO, JA; formal analysis and investigation: ZM, OS, CV, NA; writing first draft: OAP, SIO, JA; review and editing: OAP, SIO, JA; approval of final draft: OAP, SIO, JA, NA, ZM; supervision: SIO, AJ, OAP.

Funding

Open access funding provided by University of Bern.

Declarations

Conflict of interest The authors declare no competing interests.

References

Aaron J, Hungr O (2016) Dynamic simulation of the motion of partially-coherent landslides. Eng Geol 205:1–11

Aaron J, McDougall S (2019) Rock avalanche mobility: The role of path material. Eng Geol 257:105126. https://doi.org/10.1016/j.enggeo.2019.05.003

Aaron J, Wolter A, Loew S, Volken S (2020) Understanding Failure and Runout Mechanisms of the Flims Rockslide/Rock Avalanche. Front Earth Sci 8(June):1–19. https://doi.org/10.3389/feart.2020.00224

Abele G (1974) Bergstürze in den Alpen: Ihre Verbreitung, Morphologie und Folgeerscheinungen. Deutscher Alpenverein: Wissenschaftliche Alpenvereinshefte, Bd 25, 230 pp

Alfimov V, Ivy-Ochs S (2009) How well do we understand production of ^{36}Cl in limestone and dolomite? Quat Geochronol 4(6):462–474

André M (2002) Rates of postglacial rock weathering on glacially scoured outcrops (abiskoriksgränsen area, 68°n). Geogr Ann Ser A Phys Geogr 84:139–150

Argentin AL, Robl J, Prasicek G, Hergarten S, Hölbling D, Abad L, Dabiri Z (2021) Controls on the formation and size of potential landslide dams and dammed lakes in the Austrian Alps. Nat Hazard 21(5):1615–1637

Ballantyne CK, Sandeman GF, Stone JO, Wilson P (2014) Rock-slope failure following Late Pleistocene deglaciation on tectonically stable mountainous terrain. Quatern Sci Rev 86:144–157. https://doi.org/10.1016/j.quascirev.2013.12.021
Barth NC (2013) The Cascade rock avalanche: Implications of a very large Alpine Fault-triggered failure, New Zealand. Landslides. https://doi.org/10.1007/s10346-013-0389-1
Borchers B, Marrero S, Balco G, Caffee M, Goehring B, Lifton N, Nishiizumi K, Phillips F, Schaefer J, Stone J (2016) Geological calibration of spallation production rates in the CRONUS-Earth project. Quat Geochronol 31:188–198. https://doi.org/10.1016/j.quageo.2015.01.009
Calhoun NC, Clague JJ (2018) Distinguishing between debris flows and hyperconcentrated flows: an example from the eastern Swiss Alps. Earth Surf Proc Land 43:1280–1294. https://doi.org/10.1002/esp.4313
Caprez J (2008) Das Flimser Bergsturzereignis: 3D-Geländerekonstruktion und Volumenberechnung mit Hilfe von GIS. Unpubl. Master thesis, University of Zurich, pp 96
Castleton JJ, Moore JR, Aaron J, Christl M, Ivy-Ochs S (2016) Dynamics and legacy of 4.8 ka rock avalanche that dammed Zion Canyon, Utah, USA. GSA Today 26(6):4–9. https://doi.org/10.1130/GSATG269A.1
Chen R, Chen J, Xu H, Cui Z, He Q, Gao C (2022) The morphology and sedimentology of the Walai rock avalanche in southern China, with implications for confined rock avalanches. Geomorphology 413:108346. https://doi.org/10.1016/j.geomorph.2022.108346
Christl M, Vockenhuber C, Kubik PW, Wacker L, Lachner J, Alfimov V, Synal HA (2013) The ETH Zurich AMS facilities: Performance parameters and reference materials. Nucl Instrum Methods Phys Res, Sect B 294:29–38
Costa JE, Schuster RL (1988) Formation and Failure of Natural Dams. Bull Geol Soc Am 100:1054–1068
Cruden D, Hungr O (1986) The debris of the Frank Slide and theories of rockslide-avalanche mobility. Can J Earth Sci 23(3):425–432. https://doi.org/10.1139/e86-044
Davies T, McSaveney M (2012) Mobility of long-runout rock avalanches. In: Clague JJ and Stead D (eds) Landslides: Types, Mechanisms and Modeling. Cambridge University Press, pp 50–58. https://doi.org/10.1017/CBO9780511740367.006
Davies TR, McSaveney MJ (2009) The role of rock fragmentation in the motion of large landslides. Eng Geol 109:67–79. https://doi.org/10.1016/j.enggeo.2008.11.04
Deplazes G, Anselmetti FS, Hajdas I (2007) Lake sediments deposited on the Flims rockslide mass: the key to date the largest mass movement of the Alps. Terra Nova 19:252–258. https://doi.org/10.1111/j.1365-3121.2007.00743.x
Dufresne A, Bösmeier A, Prager C (2016) Sedimentology of rock avalanche deposits – Case study and review. Earth Sci Rev 163:234–259. https://doi.org/10.1016/j.earscirev.2016.10.002
Dufresne A, Davies TR (2009) Longitudinal ridges in mass movement deposits. Geomorphology 105:171–181. https://doi.org/10.1016/j.geomorph.2008.09.009
Eberle M (1987) Zur Lockergesteinsfüllung des St. Galler und Liechtensteiner Rheintales. Eclog Geol Helv 80(1):193–206
Evans JM, Stone JOH, Fifield LK, Cresswell RG (1997) Cosmogenic chlorine-36 production in K-feldspar. Nucl Instruments Methods Phys Res B 123:334–340
Evans S, Hungr O, Enegren EG (1994) The Avalanche Lake rock avalanche, Mackenzie Mountains, Northewest Territories, Canada: Description, dating and dynamics. Can Geotech J 31(5):749–768. https://doi.org/10.1139/t94-086
Fan X, Dufresne A, Subramanian SS, Strom A, Hermanns R, Stefanelli CT, Hewitt K, Yunus AP, Dunning S, Capra L, Geertsema M (2020) The formation and impact of landslide dams–State of the art. Earth Sci Rev 203:103116
Giorgio P, Consiglio NI, Ricerca R, Idrogeologica P, Verdi V (1991) Geomorphic controls of the shape and mobility of rock avalanches. October, 1365–1373
Grämiger LM, Moore JR, Vockenhuber C, Aaron J, Hajdas I, Ivy-Ochs S (2016) Two early Holocene rock avalanches in the Bernese Alps (Rinderhorn, Switzerland). Geomorphology 268:207–221. https://doi.org/10.1016/j.geomorph.2016.06.008
Hartung G (1884) Das alte Bergsturzgebiet von Flims. Zeitschr Ges Für Erdkunde Zu Berlin 19:11–194
Häuselmann P (2008) Surface corrosion of an alpine karren field: recent measurements at Innerbergli (Siebenhengste, Switzerland). Int J Speleol 37:107–111
Heim A (1883) Der alte Bergsturz von Flims. Jahrbuch Des Schweizer Alpenclub 18:295–309
Heim A (1932) Bergsturz und Menschenleben. Vierteljahresschr Naturforsch Ges Zürich 77/20, 214 pp
Hermanns RL, Longva O (2012) Rapid rock-slope failures. In: Clague JJ, Stead D (eds) Landslides: Types. Cambridge University Press, Mechanisms and Modeling, pp 59–70
Hovius N, Stark CP, Allen PA (1997) Sediment flux from a mountain belt derived by landslide mapping. Geology 25:231–234. https://doi.org/10.1130/0091-7613(1997)025<0231:SFFAMB>2.3.CO;2
Hungr O, Evans SG (2004) Entrainment of debris in rock avalanches: An analysis of a long run-out mechanism. GSA Bull 116(9/10):1240–1252. https://doi.org/10.1130/B25362.1
Hungr O, McDougall S (2009) Two numerical models for landslide dynamic analysis. Comput. Geosci. 35(5):978–992
Ivy-Ochs S, Kerschner H, Schlüchter C (2007) Cosmogenic nuclides and the dating of Lateglacial and Early Holocene glacier variations: The Alpine perspective. Quatern Int 164:53–63
Ivy-Ochs S, Poschinger AV, Synal HA, Maisch M (2009) Surface exposure dating of the Flims landslide, Graubünden, Switzerland. Geomorphology 103:104–112. https://doi.org/10.1016/j.geomorph.2007.10.024
Ivy-Ochs S, Martin S, Campedel P, Hippe K, Alfimov V, Vockenhuber C, Andreotti E, Carugati G, Pasqual D, Rigo M, Viganò A (2017) Geomorphology and age of the Marocche di Dro rock avalanches (Trentino, Italy). Quatern Sci Rev 169:188–205. https://doi.org/10.1016/j.quascirev.2017.05.014
Ivy-Ochs S, Synal HA, Roth C, Schaller M (2004) Initial results from isotope dilution for Cl and 36Cl measurements at the PSI/ETH Zurich AMS facility. Nucl Instrum Methods Phys Res, Sect B 223:623–627
Knapp S, Schwenk M, Krautblatter M (2022) Geophysical evidence of massive hyperconcentrated Bonaduz push waves with embedded Toma hills exerted by the Flims rockslide. Earth Surf Dyn. https://doi.org/10.5194/esurf-2022-20
Krietsch H, Wolter A (2018) Preliminary forensic investigation of the structural and geomorphological controls on the prehistoric Tamins rockslide in Grisons, Switzerland. In: Aversa et al. (eds.) Landslides and Engineered Slopes: Experience, Theory and Practice. Associazione Geotecnica Italiana, Rome, Italy, pp 1205–1210
Krklec K, Dominguez-Villar D, Braucher R, Perica F, Mrak I (2018) Morphometric comparison of weathering features on side bvy side carbonate rock surfaces with different exposure ages - A case from the Croation coast. Quat Int 494:275–285. https://doi.org/10.1016/j.quaint.2017.04.012
Lemaire E, Mreyen AS, Dufresne A, Havenith HB (2020) Analysis of the Influence of Structural Geology on the Massive Seismic Slope Failure Pontential Supported by Nunerical Modelling. Geosciences 10:323. https://doi.org/10.3390/geosciences10080323
Marrero SM, Phillips FM, Caffee MW, Gosse JC (2016) CRONUS-Earth cosmogenic 36Cl calibration. Quat Geochronol 31:199–219
Martin S, Campedel P, Ivy-Ochs S, Viganò A, Alfimov V, Vockenhuber C, Andreotti E, Carugati G, Pasqual D, Rigo M (2014) Lavini di Marco (Trentino, Italy): 36Cl exposure dating of a polyphase rock avalanche. Quat Geochronol 19:106–116
McDougall S, Hungr O (2004) A model for the analysis of rapid landslide motion across three-dimensional terrain. Can Geotech J 41:1084–1097. https://doi.org/10.1016/j.enggeo.2016.02.006
Müller BU (1999) Paraglacial sedimentation and denudation processes in an Alpine valley of Switzerland: An approach to the quantification of sediment budgets. Geodin Acta (Paris) 12(5):291–301
Mussina Z (2021) Deciphering the Tamins rock avalanche with cosmogenic nuclide dating, geomorphological analysis and runout modeling. Unpubl. MSc thesis ETH Zürich, 84 pp
Nabholz WK (1975) Geologischer Überblick über die Schiefersackung des mittleren Lugnez und über das Bergsturzgebiet

Ilanz-Flims-Reichenau-Domleschg. Bull Ver Schweiz Petrol Geol und –Ing 42(101):38–54
Nagelisen J, Moore JR, Vockenhuber C, Ivy-Ochs S (2015) Post-glacial rock avalanches in the Obersee Valley, Glarner Alps, Switzerland. Geomorphology 238:94–111. https://doi.org/10.1016/j.geomorph.2015.02.031
Nicolussi K, Spötl C, Thurner A, Reimer PJ (2015) Precise radiocarbon dating of the giant Köfels landslide Eastern Alps, Austria. Geomorphology 243:87–91. https://doi.org/10.1016/j.geomorph.2015.05.001
Oberholzer J (1933) Geologie der Glarner Alpen. Beiträge Geol. Karte Schweiz, N.F. 28, 626 pp
Persaud M, Pfiffner OA (2004) Active deformation in the eastern Swiss Alps: post-glacial fault, seismicity and surface uplift. Tectonophysics 385:59–84. https://doi.org/10.1016/j.tecto.2004.04.20
Pfiffner OA (1972a) Geologische Untersuchungen beidseits des Kunkelspasses zwischen Trin und Felsberg. Unpubl. Diploma thesis ETH Zürich, 171 pp
Pfiffner OA (1972b) Neue Kenntnisse zur Geologie östlich und westlich des Kunkelspasses. Eclog Geol Helv 65(3):555–562
Pfiffner OA (1977) Tektonische Untersuchungen im Infrahelvetikum der Ostschweiz. Unpubl. PhD thesis ETH Zürich/Mitt Geol Inst ETH u. Univ. Zürich, N.F| 44, 435 pp
Pfiffner OA (1978) Der Falten- und Kleindeckenbau im Infrahelvetikum der Ostschweiz. Eclogae Geol Helv 71:61–84
Pfiffner OA (2011) Structural Map of the Helvetic Zone of the Swiss Alps, including Vorarlberg (Austria) and Haute Savoie (France), 1:100'000. Geological Special Map 128, Explanatory notes
Pfiffner OA (2014) Geology of the Alps. WILEY Blackwell, 376 pp
Pfiffner OA (2022) The Flims Rock Avalanche: Structures and consequences. Swiss J Geosciences. https://doi.org/10.1186/s00015-022-00424-x
Pfiffner OA, Burkhard M, Hänni R, Kammer A, Kligfield R, Mancktelow NS, Menkveld JW, Ramsay JG, Schmid SM, Zurbriggen R (2010) Structural map of the helvetic zone of the swiss Alps. including Vorarlberg (Austria) and Haute Savoie (France), 1:100'000, Geological Special Map 128/Map sheet 5 (Panixerpass)
Pfiffner OA, Heitzmann P, Lehner P, Frei W, Pugin A, Felber M (1997) 21 Incision and backfilling of Alpine valleys: Pliocene, Pleistocene and Holocene processes. In: Pfiffner, et al. (eds) Deep Structure of the Swiss Alps: Results of NRP20, Birkhäuser, Basel, pp 265–288
Pfiffner OA, Wyss R (in press) Blatt 1195 Reichenau. Geologischer Atlas Schweiz 1:25000, Nr. 180, Erläuterungen
Piperoff C (1897) Geologie des Calanda. Beitr Geol Karte Schweiz, 7, N.F., 66 pp
Plan L (2005) Factors controlling carbonate dissolution rates quantified in a field test in the Austrian Alps. Geomorphology 68(3–4):201–212. https://doi.org/10.1016/j.geomorph.2004.11.014
Poschinger AV, Haas U (1997) Der Flimser Bergsturz, doch ein warmzeitliches Ereignis? Bull Angew Geol 2(1):35–46
Poschinger AV, Kippel T (2009) Alluvial deposits liquefied by the Flims Rock slide. Geomorphology 103(1):50–56. https://doi.org/10.1016/j.geomorph.2007.09.016
Remenyik T (1959) Geologische Untersuchung der Bergsturzlandschaft zwischen Chur und Rodels (Graubünden). Eclog Geol Helv 52(1):177–235
Rossato S, Ivy-Ochs S, Martin S, Viganò A, Vockenhuber C, Rigo M, Monegato G, De Zorzi M, Surian N, Campedel P, Mozzi P (2020) Timing, drivers and impacts of the historic Masiere di Vedana rock avalanche (Belluno Dolomites, NE Italy). Nat Hazards Earth Syst Sci 20(8):2157–2174
Ruggia G, Ivy-Ochs S, Aaron J, Steinemann O, Martin S, Rigo M, Rossato S, Vockenhuber C, Monegato G, Viganò A (2021) Reconstructing the Gorte and Spiaz de Navesele Landslides, NE of Lake Garda, Trentino Dolomites (Italy). Geosciences 11(10):404. https://doi.org/10.3390/geosciences11100404
Savage WZ (1993) Gravity-induced stresses near a vertical cliff. Int J Rock Mech min Sci Geomech Abstr 30(4):325–330. https://doi.org/10.1016/0148-9062(93)91716-V
Schälli L (2012) The diffluence of the Rhine glacier at Sargans in connection to the solid-rock surface model of the Rhine and Seez valley. Unpubl. MSc thesis Universität Zürich, pp 119
Scheidegger A (1973) On the Prediction of the Reach and Velocity of Catastrophic Landslides. Rock Mech 5:231–236
Scholz D (2018) Sedimentologische Rekonstruktion der Ausbruchsflut infolge des Flimser Bergsturzes in den potenziellen Bonaduzer See. Unpubl. MSc thesis Technische Universität München, 94 pp
Schwinner R (1912) Der Mte. Spinale bei Campiglio und andere Bergstürze in den Südalpen. PhD thesis University Zürich
Sherard JL, Woodward RJ, Gizienski SF, Clevenger WA (1963) Earth and earth-rock dams: New York, John Wiley and Sons, p 722
Singeisen C, Ivy-Ochs S, Wolter A, Steinemann O, Akçar N, Yesilyurt S, Vockenhuber C (2020) The Kandersteg rock avalanche (Switzerland): Integrated analysis of a late Holocene catastrophic event. Landslides 17(6):1297–1317. https://doi.org/10.1007/s10346-020-01365-y
Staub W (1910) Die Tomalandschaft im Rheintal von Reichenau bis Chur Jber Geogr Ges. Bern 22, 28 pp
Stone JOH, Evans JM, Fifield LK, Allan GL, Cresswell RG (1998) Cosmogenic chlorine-36 production in calcite by muons. Geochim Cosmochim Acta 62(3):433–454
Strom A (2006) Morphology and internal structure of Rockslides and Roch Avalanches: Grounds and constraints for their modelling. In: Evans SG et al (eds) Landslides from Massive Rock Slope Failure. Springer Verlag, pp 305–326
Synal HA, Bonani G, Döbeli M, Ender RM, Gartenmann P, Kubik PW, Schnabel C, Suter M (1997) Status report of the PSI/ETH AMS facility. Nucl Instrum Methods Phys Res, Sect B 123(1–4):62–68
Vockenhuber C, Miltenberger KU, Synal HA (2019) 36Cl measurements with a gas-filled magnet at 6 MV. Nucl Instrum Methods Phys Res Sect B 455:190–194. https://doi.org/10.1016/j.nimb.2018.12.046
von Wartburg J, Ivy-Ochs S, Aaron J, Martin S, Leith K, Rigo M, Vockenhuber C, Campedel P, Viganò A (2020) Constraining the Age and Source Area of the Molveno landslide Deposits in the Brenta Group, Trentino Dolomites (Italy). Front Earth Sci 8(June):1–18. https://doi.org/10.3389/feart.2020.00164
Weidinger JT, Korup O, Munack H, Altenberger U, Dunning SA, Tippelt G, Lottermoser W (2014) Giant rockslides from the inside. Earth Planet Sci Lett 389:62–73
Wildi W (1984) Isohypsenkarte der quartären Felstäler in der Nord- und Ostschweiz, mit kurzen Erläuterungen. Eclogae Geol Helv 77:541–551
Winkler S (2018) Investigating Holocene mountain glaciations: a plea for the supremacy of glacial geomorphology when reconstructing glacier chronologies (supported by an example from the Southern Alps/New Zealand). Erdkunde 72(3):215–234
Wolters G, Müller G (2008) Effect of cliff shape on internal stresses and rock slope stability. J Coastal Res 24(1):43–50. https://doi.org/10.2112/05-0569.1
Zeng Q, Zhang L, Davies T, Yuan G, Xue X, Wie R, Yin Q, Liao L (2019) Morphology and inner structure of Luanshibao rock avalanche in Litang, China and its implications for long-runout mechanisms. Eng Geol 260:105216. https://doi.org/10.1016/j.enggeo.2019.105216
Zwahlen P (2021) Geologie des Alpenrheintales Terra Plana 2:4–13

O. Adrian Pfiffner (✉) · Naki Akçar
Institute of Geological Sciences, University of Bern, Bern, Switzerland
Email: adrian.pfiffner@geo.unibe.ch

Susan Ivy-Ochs · Olivia Steinemann · Christof Vockenhuber
Laboratory of Ion Beam Physics, ETH Zurich, Zurich, Switzerland

Zhasmin Mussina · Jordan Aaron
Geological Institute, ETH Zurich, Zurich, Switzerland

Jordan Aaron
Swiss Federal Institute for Forest, Snow and Landscape Research WSL, Birmensdorf, Switzerland